May 2022

Effect of 670 Nm Photobiomodulation on Angiogenic and Inflammatory Signaling Pathways in an in Vitro Model of Diabetic Retinopathy

Annamarie Grace Lofald
University of Wisconsin-Milwaukee

Effect of 670 nm photobiomodulation on angiogenic and inflammatory signaling pathways in an *in vitro* model of diabetic retinopathy

by

Annamarie Lofald

A Thesis Submitted in

Partial Fulfillment of the

Requirements for the Degree of

Master of Science

in Biomedical Sciences

at

The University of Wisconsin – Milwaukee

May 2022

ABSTRACT

Effect of 670 nm photobiomodulation on angiogenic and inflammatory signaling pathways in an *in vitro* model of diabetic retinopathy

by
Anna Lofald

The University of Wisconsin – Milwaukee, 2022
Under the Supervision of Elizabeth Liedhegner, Ph.D.

Approximately 1 in 10 Americans suffers from diabetes mellitus, and the frequency escalates to 1 in 4 for individuals over 65 years of age (Centers for Disease Control and Prevention, 2020). These statistics are jarring considering the absence of a cure forces patients to endure lifelong physician supervised disease management or increase their risk of developing vascular complications. Alas, even patients able to obtain world-class research informed treatments and lifestyle advice may still be afflicted with macrovascular and microvascular dysfunction as the disease progresses. Insulin deficiency and resistance leads to metabolic dysregulation and fosters an environment saturated with glucose due to insufficient hormone-mediated translocation into adipose and muscle tissue *(Wilcox, 2005)*. Hyperglycemia coincides with dyslipidemia, mitochondrial dysfunction, and aberrant cellular signaling with devastating consequences including the most common microvascular consequence, diabetic retinopathy (DR). Importantly, exposure to high glucose directly is not the sole source of cellular distress in DR, but, rather, downstream signaling initiated by excessive blood sugar induces chronic inflammation and expression of angiogenic factors that contribute to pathogenic growth of widespread yet poorly constructed vessels that often advance into ocular pathologies and severely threaten a patient's vision *(Busik, Mohr, & Grant, 2008)*. Far red/near-infrared (R/NIR) photobiomodulation (PBM) is a non-invasive therapy that has been shown to ameliorate inflammatory mediators and stabilize mitochondrial activity in several animal and cell culture disease models, including DR. Accordingly, ***we hypothesized that light therapy at 670 nm will enhance expression***

of anti-angiogenic proteins and attenuate high glucose-induced mediators of inflammation in a rat retinal Müller cell model of diabetic retinopathy. This hypothesis was tested with the following the following focuses. **Specific aim 1:** Identify expression of anti-angiogenic proteins under high glucose conditions in a cultured Müller cell model of diabetic retinopathy and when treated with 670 nm PBMT. **Specific aim 2:** Identify inflammatory and angiogeneic cytokines expressed under high glucose conditions in a cultured Müller cell model of diabetic retinopathy and determine the effect of 670 nm PBMT. **Research objective:** This study will evaluate whether inflammatory and angiogenic mediators affected by high glucose can be attenuated with PBM to further enhance understanding of the technology and its potential to treat DR patients. **Results:** We found that high glucose mildly, if at all, affects TSP-1 expression within and secreted by Müller cells (MCs). In addition, 670 nm PBM tends to increase expression of TSP-1 within and secreted by MCs. These findings suggest trends but lack significance ($p<0.05$). We were unable to visualize TGF-β due to serum interference. Similarly, unanticipated assay limitations prevented quantification of IL-1β, IL-6, IL-10, and TNF-α in Müller cell conditioned media as sample concentration measurements failed to fall within the standard curves.

TABLE OF CONTENTS

LIST OF FIGURES & TABLES

LIST OF SUPPLEMENTARY FIGURES & TABLES

LIST OF ABBREVIATIONS

AGE	Advanced glycation end products
BRB	Blood retinal barrier
CcO	Cytochrome c oxidase
CDC	Center for Disease Control
DM	Diabetes mellitus
DME	Diabetic macular edema
DMEM	Dulbecco's Modified Eagle Medium
DR	Diabetic retinopathy
DTT	Dithiothreitol
EC	Endothelial cell
ELISA	Enzyme-linked immunosorbent assay
FBS	Fetal bovine serum
HG	High glucose
HREC	Human retinal endothelial cells
ICAM-1	Intracellular adhesion molecule-1
IL-1β	Interleukin-1 beta
IL-1RA	Interleukin-1 receptor agonist
IL-6	Interleukin-6
IL-10	Interleukin-10
LAP	Latent-associated peptide
LED	Light-emitting diode
MC	Muller cells
MIO-M1	Immortalized human Muller cell line
MMP	Matrix metalloproteinase
N	Normal glucose
NO	Nitric oxide
NPDR	Non-proliferative diabetic retinopathy
OC	Osmolarity control
PBM	Photobiomodulation
PDR	Proliferative diabetic retinopathy
PEDF	Pigment epithelium-derived factor
PVDF	Polyvinylidene fluoride
qPCR	Quantitative PCR
rMC-1	Immortalized rat Muller cell line
R/NIR	Far red/near-infra red
ROS	Reactive oxygen species
RPE	Retinal pigment epithelium
SDS-PAGE	Sodium dodecyl sulphate-polyacrylamide gel electrophoresis
STZ	Streptozotocin
T1D	Type 1 diabetes
T2D	Type 2 diabetes
TGF-β	Transforming growth factor beta
TNF-α	Tumor necrosis factor alpha
Treg	Regulatory T cells
TSP-1	Thrombospondin-1
TBST	Tris buffered saline
VEGF	Vascular endothelial growth factor

ACKNOWLEDGEMENTS

An achievement of this magnitude cannot be accomplished alone. After inception of the study, Dr. Liedhegner and Dr. Eells supported the project from the preliminary literature dive to the frustrating setbacks. Their leadership was irreplaceable. Despite isolating circumstances of the 2020 pandemic, I never felt alone in my work. I must also acknowledge that the seed of inspiration for this project was heavily influenced by the fascinating notion of cell-cell communication covered in Dr. Nardelli's immunology courses. Finally, thank you to my parents for encouraging me to ask questions about the world; stifled curiosity could not have resulted in penning the following paper.

INTRODUCTION

Diabetes mellitus

Diabetes mellitus (DM) is a relatively common metabolic and endocrine disorder affecting the body's capacity to regulate blood glucose levels. It remained a fatal concern until the 20th century with discovery and isolation of the pancreatic hormone responsible for regulating glucose metabolism, insulin. In addition to this Nobel prize winning breakthrough, numerous scientific advancements have transformed diabetes from an often-lethal disease to one that is manageable with proper education and medical guidance. According to a 2020 report from the Centers for Disease Control and Prevention (CDC), over 10% of the American population is presumed to have diabetes mellitus due to pathologic insulin deficiency (type I diabetes; T1D) or acquired insulin resistance (type II diabetes; T2D) *(Centers for Disease Control and Prevention, 2020)*. Type II DM accounts for the majority of DM cases and is a growing public health concern due to its correlation with rising obesity rates.

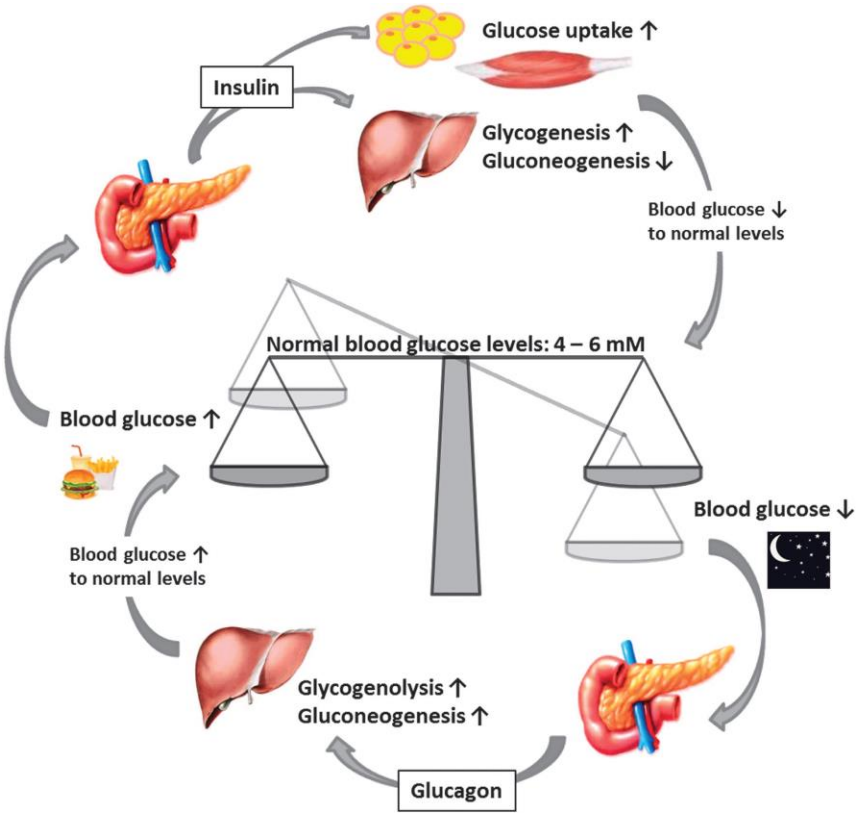

Figure 1: Normal regulation of blood glucose *(Roder, et al. 2016)*

In a non-diseased system, blood glucose concentration is regulated by two main pancreas-derived hormones. Insulin and glucagon work opposite one another to decrease or increase blood glucose, respectively, to maintain a normal concentration within the range of 4—6 mmol/L *(Goke, 2008) (Komatsu, Takei, Ishii, & Sato, 2013)* (***Figure 1***). Glucose levels rise after a meal is consumed and digested, releasing carbohydrates into the bloodstream. A subset of pancreatic cells responds to this imbalance by secreting insulin. Some cells have a naturally high demand for energy or capacity for storage (e.g., muscle or adipose tissues) *(Zisman, et al., 2000) (Kohn, Summers, Birnbaum, & Roth, 1996)*. Glucose normally enters these tissues via transporter channels that open upon contact with insulin (Saltiel & Kahn, 2001). In diabetic patients, insulin does not effectively open glucose transporters and excess sugar remains in the blood. When the body fails to open channels necessary for directing glucose to cells with mechanisms able to tolerate a sugary assault, cells such as those constructing the adjacent vasculature that are metabolically incapable of disposing of overwhelming sugar suffer dysfunction and eventually accumulate damage.

DM is a polygenic disorder that is likely influenced by environmental factors, though the etiology is incompletely defined. Select autoantibodies may be used to diagnose the disease as it is a result of inappropriate autoimmune reactivity in some cases, but disease presentation in other patients is idiopathic. Bodily damage as a consequence of chronic hyperglycemia, among other dysregulated mechanisms, accumulates with disease progression and may lead to macrovascular complications such as heart disease or stroke. Elevated blood glucose also disrupts anatomical locations that lack mechanisms to shield excessive cellular uptake of the sugar molecule, such as

peripheral nerves, renal glomeruli, and the retina. This leads to corresponding microvascular complications including neuropathy, nephropathy, and retinopathy, respectively.

Diabetic Retinopathy

Despite decades of innovation, diabetic patients face a lifelong obligation to monitor and modulate circulating glucose levels, and still frequently develop vascular complications. Research suggests that roughly 30 types of ocular cells are affected by diabetes *(Stitt, et al., 2016)*, so it is unsurprising that diabetic retinopathy (DR) was determined to be the most common microvascular complication *(Antonetti, Klein, & Gardner, Diabetic retinopathy, 2012)*. Over half of T2D patients and virtually all T1D patients develop DR *(Klein, Klein, & Moss, 1989)* due to functional consequences compounding throughout the patients' lives which is not only a health risk, but also a financial burden because healthcare costs associated with DM double when faced with managing this concerning microvascular complication *(Heintz, Wirehn, Bourghardt Peebo, Rosenqvist, & Levin, 2010)*.

At present, there is a lack of therapeutic treatments available to wholly prevent or treat the source of DR since the pathology is multi-factorial and incompletely understood. Therefore, therapies to attenuate the dysregulation that cumulates are in high demand. The disease may manifest as non-proliferative diabetic retinopathy (NPDR) causing macular edema, or proliferative diabetic retinopathy (PDR), resulting in aberrant blood vessel growth known as angiogenesis. DR is the leading cause of blindness in adults and will continue to be a pervasive

issue due to the steadily rising prevalence of DM in the population as a consequence of lifestyle and diet changes made in the last century *(Eden & Klein, 2007)*.

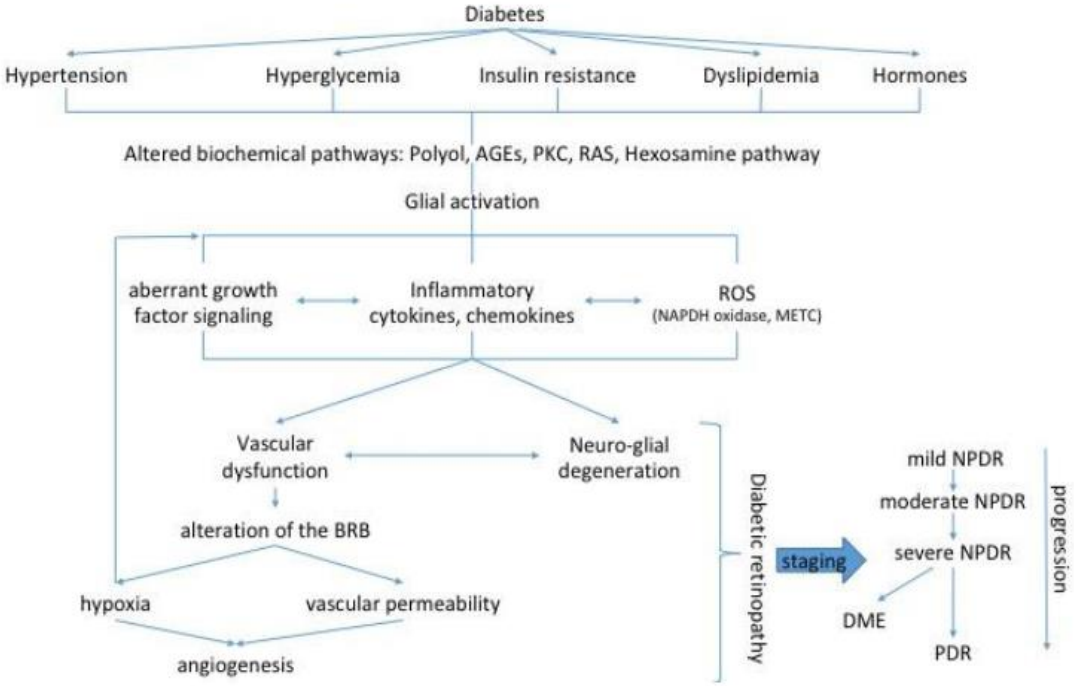

Figure 2: Pathogenic dysregulation due to diabetes mellitus *(Rubsam, et al., 2018)*

Chronic hyperglycemia affects cells by increasing endogenous oxidative stress and reactive oxygen species (ROS), including superoxide anions, hydroxyl radicals, and hydrogen peroxide. Additionally, mitochondrial function is often impaired, though it remains to be elucidated which mechanism precedes the other. These stressors prompt pathogenic upregulation of signaling cascades including the polyol pathway, hexosamine pathway, protein kinase C pathway, and the advanced glycation end products (AGE) pathway *(Brownlee, 2005)* (***Figure 2***). Mitochondrial damage or dysfunction reduces the organelle's efficiency, and impaired respiration results in excessive intracellular ROS and intensifies compounding of oxidative stress.

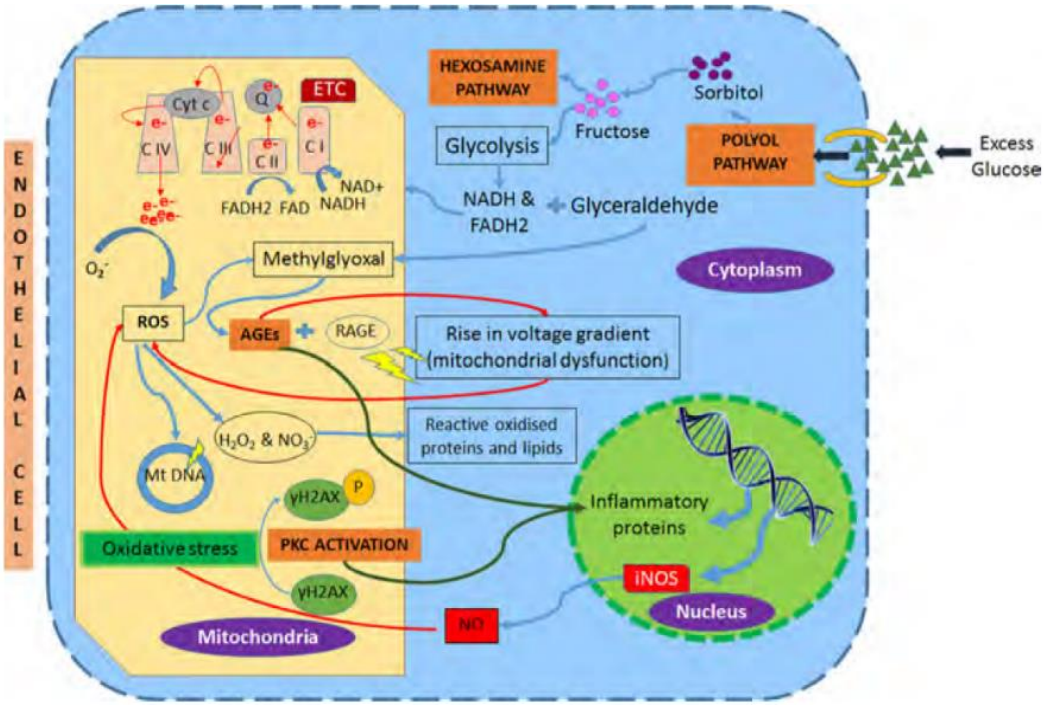

Figure 3: Cellular dysfunction due to hyperglycemia *(Stitt, et. al., 2016)*

Inflammation is posited to be the main mechanism of vascular endothelial cell (EC) injury, as opposed to damage caused directly as a result of high glucose concentrations. Busik et al. (2008) demonstrated that human retinal endothelial cells (HRECs) initiated injurious mechanisms such as elevated glucose consumption and mitochondrial superoxide production when induced with the inflammatory cytokines IL-1β and TNF-α but not with exposure to excessive glucose alone, suggesting paracrine signaling as a main source of dysfunction *(Busik, Mohr, & Grant, 2008)*. Extracellular toxicity related to EC destruction accumulates, leading not only to further cellular degeneration and leakage of fluids from compromised vessel junctions, but also to activation of compensatory mechanisms to repair the damaged vasculature (***Figure 3***).

Angiogenesis arises when pro-angiogenic factors begin to outweigh the presence of anti-angiogenic factors, therefore initiating new vessel growth tangential to existing vasculature. Despite this process ostensibly functioning to mend the damage, adverse effects of vascular expansion are not uncommon. Neither formation of new blood vessels nor clotting measures to prevent ischemic leakage from the damaged tissue (i.e. blood-retinal-barrier [BRB], capillaries, arterioles) occur instantaneously, thus fluid inevitably escapes into the intraretinal space. In advanced stages of DR, angiogenic ischemia may progress into diabetic macular edema (DME) and is the prominent cause of blindness in DR patients *(Zhang, Zeng, Bao, Wang, & Gillies, 2014)*.

Ocular anatomy and physiology

Numerous cell types populate the vertebrate eye and form what has been termed the neurovascular unit, such that retinal neurons that transmit electrochemical signals paramount for sight are distinctly surrounded by supporting cells and the necessary vasculature (***Figure 4***). Light in the form of photons, a type of massless quantum particle, crosses the cornea, lens, and vitreous humor before broaching the retina. Five types of retinal neurons – amacrine cells, bipolar cells, ganglion cells, horizontal cells, and photoreceptors (e.g., rods and cone) – refine and direct the electrochemical signals to the optic nerve in established pathways depending on the stimuli and external conditions. Retinal glia – Müller cells (MCs), astrocytes, and microglial cells – are a separate category of cells responsible for clearing debris, providing structural stability, and participating in eye-specific immune surveillance. To complete the neurovascular unit,

oxygen and other essential nutrients are delivered to the eye via blood vessels comprised of vascular ECs encased in pericytes, or smooth-muscle cells, to regulate the rate of blood flow.

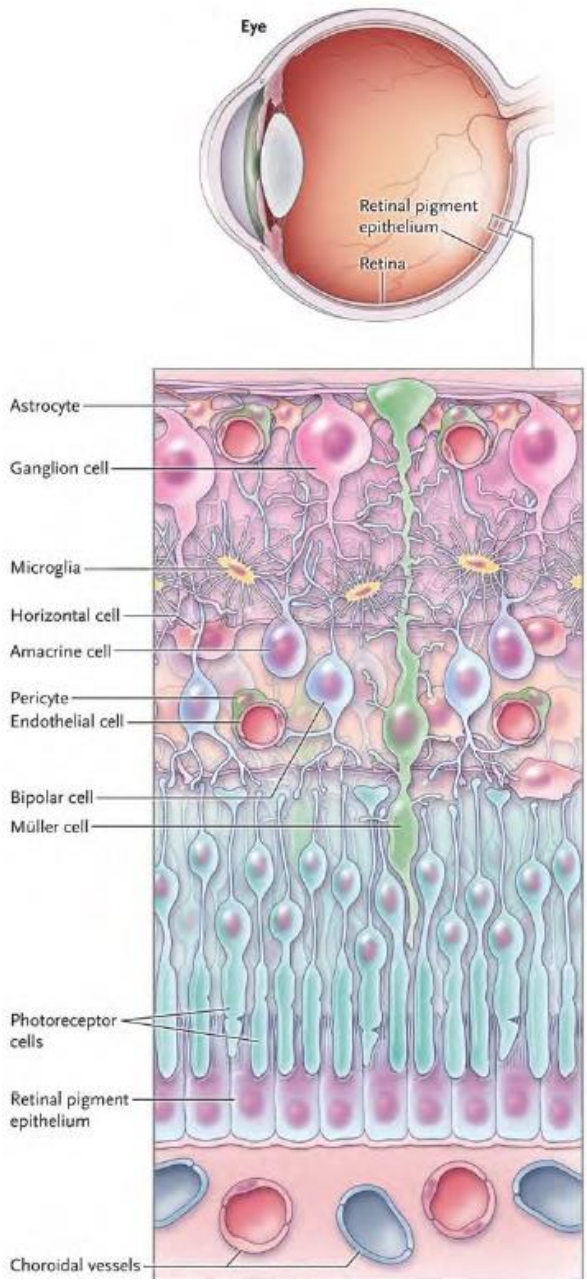

Figure 4: The retinal neurovascular unit *(Antonetti, et. al., 2012)*

The eye has been characterized as one of the body's few immune-privileged locations. Immune cell access to the organ is limited by mechanistic and structural barriers such as the retinal pigment epithelium (RPE) that prevent ubiquitous exposure to environmental antigens from inciting an inflammatory response. This elite status is fortified by the BRB, comprised of ECs, astrocytes, pericytes, and MCs. Ocular cells may be diverse, but overlapping roles and responsibilities generally protect the eye from slight alterations such as temporary metabolic disturbances. In DR, the organ function wanes because tremendous systemic dysfunction cannot be mitigated even with all cells extending their capabilities. Neurons are not naturally regenerative, so functional damage is regarded as permanent.

Müller glial cells

Glial cells support and maintain homeostasis of the neurovascular unit by phagocytosing debris and providing neurotrophic factors that regulate neural survival. They can be further sorted into microglia and macroglia. Since typical circulating immune cells lack the ability to access the eye due to strict regulation of the BRB, microglia serve as the primary resident cells responsible for ocular immunity. Alternatively, MCs, the main macroglial cell population, are far more abundant and functionally diverse. Transgenic modification of rats allowed researchers to selectively eliminate MCs and deduce their role from the resulting systemic consequences. Experimental results suggested that glial dysfunction may be correlated to neurodegeneration, BRB breakdown, photoreceptor damage and reduced functional capacity, and vascular effects in ocular pathologies including DR *(Shen, et al., 2012)*.

MCs function to support and protect neurons in various ways, including storing excess glucose as glycogen when the body is hyperglycemic and redistributing stored energy substrates to the environment during scarcity. MCs are the primary glial cells in vertebrates and traverse the retina almost entirely as they extend through six distinct retinal layers, from the inner to outer limiting membranes, as well as physically participating in formation and maintenance of exterior membranes *(Coorey, Shen, Chung, Zhu, & Gillies, 2012)* and the BRB (*Hosoya & Tomi, 2005*). The size and broad distribution of MCs provides structure for the retina in addition to allowing molecular exchange and communication between the wide variety of cell types dispersed in retinal tissues, including components of vascular beds (e.g., ECs, pericytes) and photoreceptors

(e.g., rods, cones) *(Bringmann, et al., 2006)* (***Figure 5***). Unfortunately, MCs cannot respond to stressors in a layer-specific manner *(Vecino, Rodriguez, Ruzafa, Pereiro, & Sharma, 2016),* which suggests that biochemical assault to the retina threatens MC dysfunction.

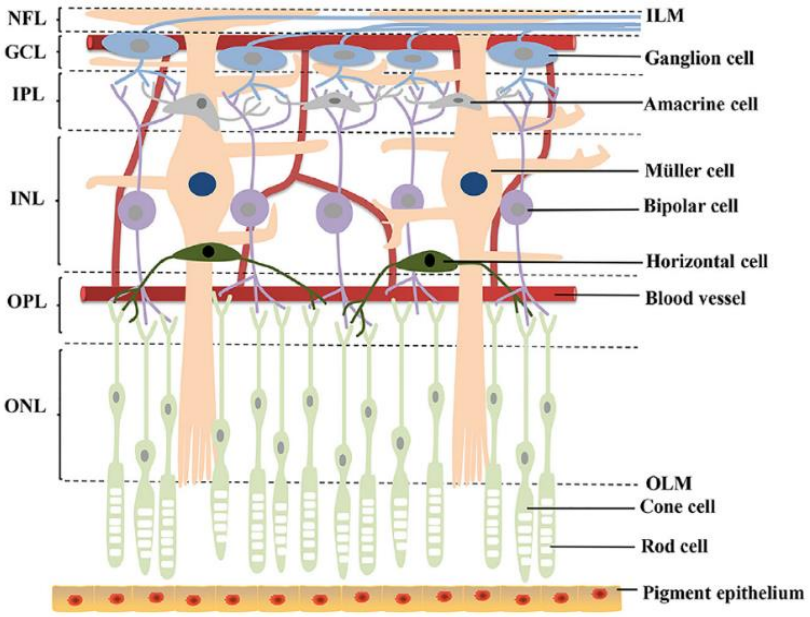

***Figure 5**: **Schematic of cell types comprising retinal layers** (Li, et. al., 2019)*

These multi-purpose cells are relevant in the present study because hyperglycemia in DR induces MC dedifferentiation *(Hosoki, et al., 2015)* and apoptosis *(Feenstra, Yego, & Mohr, 2013)*. Loss of these integral cells contributes to detrimental breakdown of the BRB, compromises vascular integrity, and induces neuronal dysfunction and death *(Shen, et al., 2012)*. MCs also have a role in inflammation that is noted in DR patients. High glucose (HG) induces transcription of inflammatory response genes as seen in primary MCs from streptozotocin-induced diabetic rats, including those involved in antigen presentation, cell adhesion, signal transduction, and transcriptional regulation *(Gerhardinger, et al., 2005)*. Importantly, MCs participate in maintaining an anti-proliferative environment for vascular ECs. Dysregulation of MCs may offset the homeostatic balance of pro- and anti-angiogenic factors, and pathogenic blood vessel growth enhances ocular damage in DR (***Figure 6***).

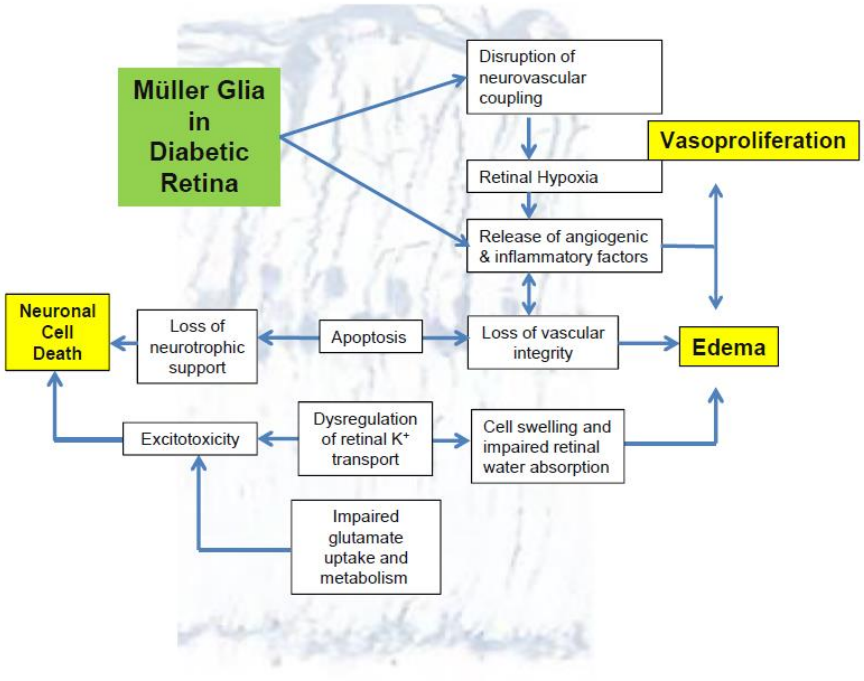

Figure 6: Role of Muller glial cells in diabetic retinopathy *(Stitt, et. al., 2016)*

Current DR treatments

Presently, there is a lack of effective preventative treatments for DR despite continued evaluation of the use of insulin supplementation or regulation protocols, diet modifications, and monoclonal antibodies. Intraretinal injection of the humanized monoclonal antibody anti-vascular endothelial growth factor (VEGF) is especially important for PDR patients because rampant VEGF-induced angiogenesis is the primary source of excessive vessel proliferation *(Witmer, Vrensen, Van Noorden, & Schlingemann, 2003) (Wang, Wang, & Wang, 2009)*. Three types of anti-VEGF therapies have been introduced, though only two have been awarded FDA approval to treat DR and pose risks such as increased intraocular pressure or inflammation (i.e., uveitis). The antibodies have varying half-lives, and some target multiple VEGF isoforms while others are more limited. While the antibodies specifically neutralize VEGF activity, VEGF is anatomically abundant.

Consequently, diffusion of the injection to other areas of the body may lead to vascular complications where unaltered activity of VEGF is necessary *(Zhao & Singh, 2018)*. Therapies are also scant for patients after the onset of disease, but the prominent DR treatment is laser photocoagulation. This non-invasive technology focuses a 400 – 700 nm laser on the choroid and RPE where the light generates heat to sacrifice some cells in an effort to treat and prevent further angiogenic degeneration. Studies support a decrease in VEGF and regression of neovascularization following treatment *(Aiello, et al., 1994)*. Due to the mechanism relying on calculated destruction, patients are still subject to risks such as cataract formation, corneal burns, hemorrhaging, exacerbated macular edema, and reduced dark field, color, or peripheral vision (Gr*aham, Binz, Shen, Constable, & Rakoczy, 2006) (Shimura, et al., 2003)*.

Photobiomodulation

Mounting evidence supports that photobiomodulation (PBM), also termed light therapy, could be a non-invasive and low risk addition to the short list of DR treatments. This technique works by introducing light at a precise wavelength to superficial tissue via laser or a light emitting diode (LED) array, often over several sessions, with the goal of restoring dysregulated internal biological mechanisms. Instead of inciting measured annihilation via a heat-induced mechanism to limit potentially exacerbated future damage as is the goal of laser photocoagulation, PBM is posited to operate by stimulation of intracellular pigmented molecules called chromophores with directed light waves. Chlorophyll in plants is a well-known chromophore that absorbs red and blue light emitted by the sun for photosynthesis, but a myriad of light-absorbing molecules exists in animals, as well, including hemoglobin, flavins, and cytochrome c oxidase (CcO) *(Karu, 1999)*.

Though it is understood light therapy induces a photochemical mechanism, it remains unclear precisely which molecular target or targets and consequent signal transducing pathways are modified.

Decades of light therapy research demonstrate a biphasic dose response to treatment; low doses of PBM enhance cellular bioenergetics while high doses cause inhibition. DR studies favor light within the far-red to near-infrared (R/NIR) range (600 – 1100 nm) due to mammalian ocular anatomy. These longer wavelengths are compatible with diffraction through superficial components of the eye, whereas blue or green light (450 – 560 nm) scatter upon intersection with tissue to such a degree that light is not effectively focused on the interior target (i.e., retina). Assessment of action spectra of probable chromophores suggests modified activity of CcO, complex IV in mitochondrial respiration and an essential enzyme for electron transport (***Figure 7***). Karu and Kolyakov (2005) identified four peaks in the PBM action spectrum, one of which closely corresponds with that of CcO, positioning this enzyme as a feasible target. Repeated light therapy application at R/NIR wavelengths generally results in increased mitochondrial

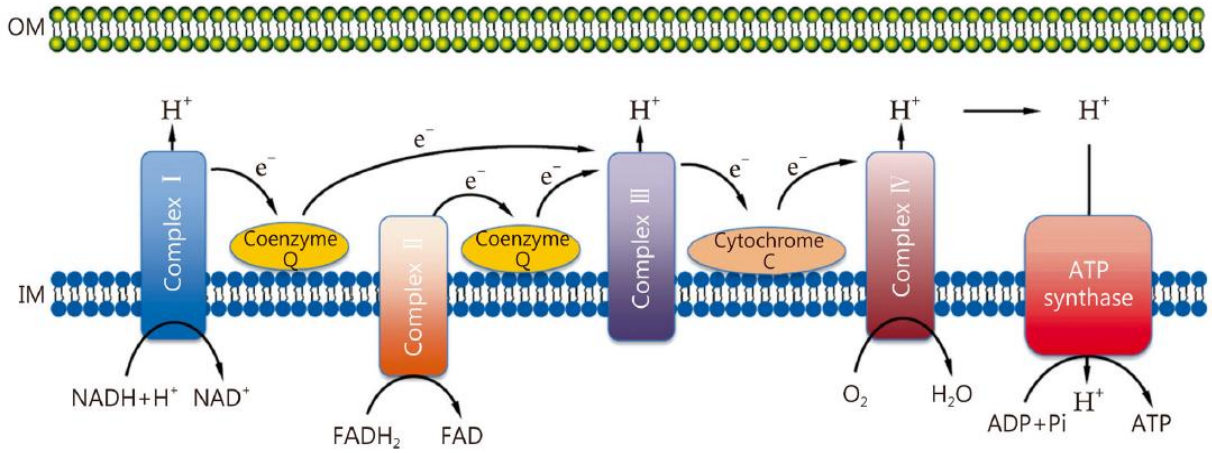

Figure 7: Functional components of the electron transport chain *(Zhang, et. al., 2018)*

respiration, oxygen consumption, electron transport, and ATP production in addition to activation of many transcription factors and reduced cumulative oxidative stress. To assert PBM in the context of other treatment regimens, Huang et al. (2009) described the parameters for irradiation (i.e. wavelength [nm], power density [W/cm^2]) as the "medicine," while the application specifications (i.e. energy density [J/cm^2], time [sec], interval [treatment frequency]) are equivalent to the medicinal "dose."

Ample evidence supports that R/NIR light therapy can reduce diabetes-induced production of ocular ROS and inflammation and restore mitochondrial function affected by hyperglycemic conditions. Insufficient treatment options for DR patients and the possibility that PBM could mitigate direct and indirect consequences of chronic hyperglycemia drive continued research of light therapy technology in the framework of DM. Multiple diabetic animal models have been developed for research purposes. One such model generates animals with systemic consequences comparable to DM patients by injecting Streptozotocin (STZ), a substance toxic to insulin-producing cells. When STZ-induced mice *(Saliba, et al., 2015)* or rats *(Tang, et al., 2013)* were treated with several sessions of 670 nm light, the rodents exhibited reduced superoxide production, ICAM-1 expression, leukostasis (vascular extravasation of white blood cells), and inflammation. These alterations coincided with attenuated disease severity in the animals and were mirrored in murine retinal cell cultures. Subsequent experimentation by the latter lab examined four human patients with T2D and non-center involving DME, a potential consequence of DR. Only one eye of each participant received the bidaily 670 nm LED treatment while the opposite eye served as a control. Researchers noted that macular thickness continued to increase

in the control eye while the macular thickness decreased in all treated eyes including in the patient that opted to discontinue in the study after 2 months, in contrast to 9 months of treatment experienced by the remaining 3 participants *(Tang, Herda, & Kern, 2014)*.

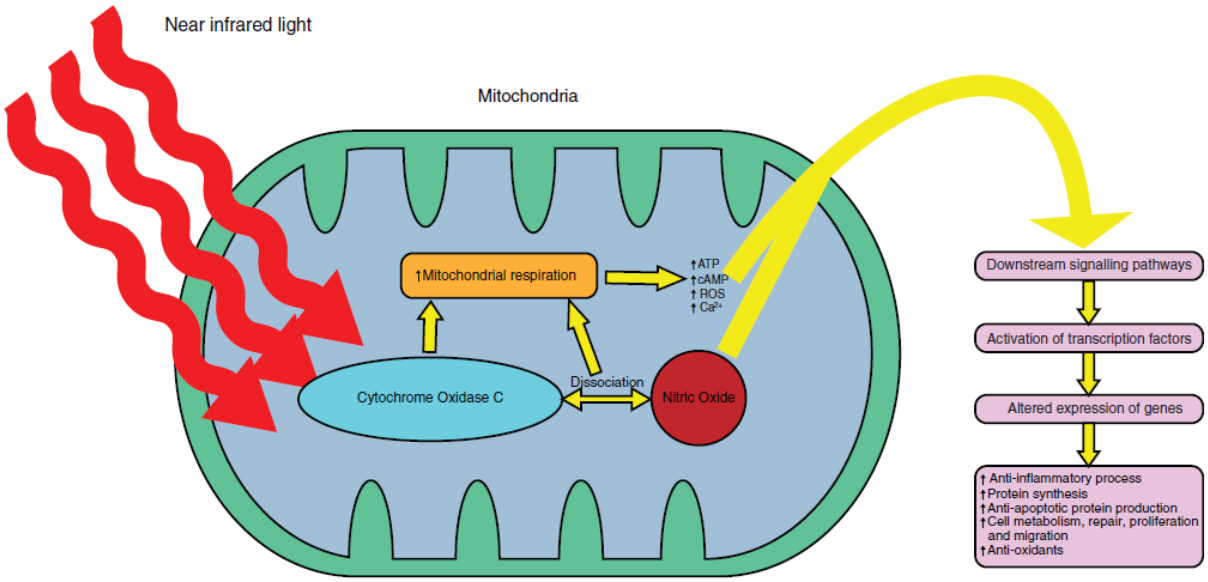

***Figure 8**: **Proposed mechanism of photobiomodulation for near infrared light wavelengths (630-1000nm)** (Ao, et. al., 2018) Near infrared light targets the mitochondrial enzyme cytochrome oxidase C resulting in (i) direct stimulation in mitochondrial respiration and (ii) dissociation of nitric oxide which indirectly increases mitochondrial respiration.*

Although the complete mechanism for PBM has not yet been elucidated, some theories prevail, as no data has entirely validated or eliminated them as contenders. Perhaps the most prominent theory proposes that CcO is indeed the target chromophore. According to this theory, heme and copper non-covalently interpolated within the enzyme associate with the metabolically inhibiting free radical nitric oxide (NO) during impaired mitochondrial respiration, and PBM induces dissociation of this molecule so that it can be replaced with oxygen *(Lane, 2006)* (***Figure 8***). Indeed, this could explain increased tissue oxygenation seen in PBM studies. Additionally, a study from Eells et al. (2003) demonstrated that 670 nm red light therapy significantly improved

neuronal function in rats intoxicated with methanol, a substance known to inhibit cytochrome oxidase activity. This supports that complex IV of the electron transport chain is indeed directly affected by R/NIR PBM. Regardless of mechanistic intricacies, the downstream therapeutic effects of PBM have been well-characterized and support further exploration of this technology.

SUMMARY AND GAP IN KNOWLEDGE

The prognosis and treatment of DM has changed radically since the discovery and refinement of glucose regulating practices; however, vascular complications remain common even among patients with the privilege of access to leading medical professionals and technology. In a non-diseased individual, regulation of blood glucose is a dynamic, autonomic process characterized by disseminating the appropriate amount of insulin based on the concentration of sugar detected *(Saltiel & Kahn, 2001)*. Diabetic patients lack either insulin or insulin sensitivity, but the primary concern in both scenarios is lack of glucose transport out of the blood. Consequently, cells lining the vasculature suffer repeated glycemic assault which may evolve into targeted vascular complications. Persistent ocular hyperglycemia leads to increased inflammatory signaling and aberrant growth of new blood vessels which contribute to the mechanism of vision loss experienced by many diabetic patients. Studies suggest that diabetic retinopathy is the leading microvascular complication among diabetic patients, yet no effective, non-invasive, and affordable treatment is available *(Antonetti, Klein, & Gardner, Diabetic retinopathy, 2012)*.

The present study investigated the notion that photobiomodulation, specifically red-light therapy, may be a non-invasive technique that could induce positive biological changes (e.g.,

modified protein expression) within the neurovascular unit for patients suffering from diabetic retinopathy. The research focused on a single yet significant subset of retinal glial cells, Müller cells, as they are abundant and extend between five of the approximately seven anatomically defined layers of the retina. This information paired with studies confirming that Müller cells indeed produce the proteins associated with inflammation and angiogenesis suggest it is reasonable to imagine that the activity of this cell type could influence the status of the surrounding environment *(Eastlake, et al., 2016) (Eichler, Yafai, Wiedemann, & Reichenbach, 2004) (Gerhardinger, et al., 2005)*.

All in all, two questions were posed. First, how does prolonged high glucose affect expression of certain inflammation and angiogenesis-associated proteins in Müller cells? Second, could hyperglycemia-induced changes to protein expression be ameliorated with light therapy?

HYPOTHESIS AND SPECIFIC AIMS

Approximately 1 in 10 Americans suffers from diabetes mellitus, and the frequency escalates to 1 in 4 for individuals over 65 years of age *(Centers for Disease Control and Prevention, 2020)*. These statistics are jarring considering the absence of a cure forces patients to endure lifelong physician-supervised disease management or increase their risk of developing vascular complications. Alas, even patients able to obtain world-class research-informed treatments and lifestyle advice may still be afflicted with macrovascular and microvascular dysfunction as the disease progresses. Insulin deficiency and resistance leads to metabolic dysregulation and fosters an environment saturated with glucose due to insufficient hormone-mediated translocation into

adipose and muscle tissue *(Wilcox, 2005)*. Hyperglycemia coincides with dyslipidemia, mitochondrial dysfunction, and aberrant cellular signaling with devastating consequences including the most common microvascular consequence, diabetic retinopathy. Importantly, exposure to high glucose directly is not the sole source of cellular distress in DR, but, rather, downstream signaling initiated by excessive blood sugar induces chronic inflammation and expression of angiogenic factors that contribute to pathogenic growth of widespread yet poorly constructed vessels that often advance into ocular pathologies and severely threaten a patient's vision *(Busik, Mohr, & Grant, 2008)*. R/NIR PBM is a non-invasive therapy that has been shown to ameliorate inflammatory mediators and stabilize mitochondrial activity in several animal and cell culture disease models, including DR. Accordingly, we hypothesized that light therapy at 670 nm will enhance expression of anti-angiogenic proteins and attenuate high glucose-induced mediators of inflammation in a rat retinal Müller cell model of diabetic retinopathy.

Specific Aim 1: **Identify expression of anti-angiogenic proteins under HG conditions in a cultured MC model of DR compared to MCs treated with 670 nm PBM**. Our working hypothesis was that expression of these proteins will be elevated under hyperglycemic conditions and will be further increased after exposure to an LED array at 670 nm. Disruption to the ocular environment that favors vascular expansion is a recognized consequence of glycemic stress. Some pro-angiogenic mediators are established threats to the delicate balance (e.g., VEGF), so elevated transcription of these functionally opposite proteins when under cellular duress could be a compensatory mechanism. Attenuated disease progression with PBM has been reported in patients and animal models, suggesting a restoration of angiostasis. PBM's ability to reestablish

a healthy equilibrium would require an increase in pro-angiogenic proteins, a decrease in anti-angiogenic proteins, or, realistically, a combination of the processes.

Specific Aim 2: Determine efficacy of 670 nm PBM treatment at mitigating expression of cytokines associated with inflammation in a cultured MC model of DR. Our working hypothesis was that hyperglycemic conditions would induce inflammatory cytokine signaling that will be attenuated with 670 nm PBM. A number of studies report a link between high glucose and increased ocular inflammation. Many inflammatory cytokines derive from activation of the transcription factor NF-κB, and previous work from this lab reported a PBM-induced reduction in NF-κB activity. Therefore, we speculated a decrease in transcription of downstream inflammatory proteins as a result of light therapy.

We examined how expression of inflammatory and angiogenic mediators modified by hyperglycemic conditions are altered with PBM. Experimentation using a cellular model of DR generated data with the intention of informing researchers and clinicians of the therapeutic potential for this non-invasive technology.

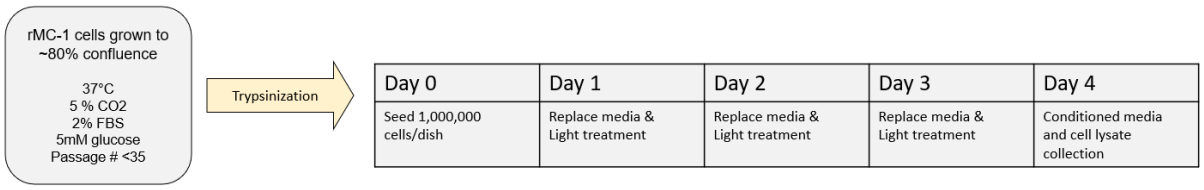

Figure 9: Culturing conditions and temporal distribution of cell maintenance, seeding, and sample collection

MATERIALS AND METHODS

Model System: Experiments were performed on the immortalized rat retinal Müller glial cell line, rMC-1. MCs maintain physical contact with virtually every type of retinal cell including those of the ocular vasculature and foundational RPE *(Bringmann, et al., 2006)*. The central location, abundant distribution, and expansive role of MCs in the retina positioned them as suitable candidates to examine dysregulated cellular signaling in DR. Frozen Müller cells were graciously gifted to the Eells lab from John Mieyal, Case Western Reserve University. Were cultured in 100 mm polystyrene dishes at 37°C/5 % CO_2 with 10 mL of either high (25 mM) or normal (5 mM) D-glucose in Dulbecco's Modified Eagle Medium (DMEM) (Invitrogen 11995 and Invitrogen 11885, respectively). Alternatively, mannitol (20 mM), a non-glucose sugar, was dissolved in normal (5 mM) D-glucose DMEM (Invitrogen 11885) to create the third variation of culture media with the purpose of controlling for osmolarity. All culture medium was supplemented with 2% heat-inactivated fetal bovine serum (FBS) (Corning 35011CV) and 1% penicillin/streptomycin (Gibco 15140122). Day 0, one day preceding the first light treatment, cell density calculations were performed on cells trypsinized and suspended in media to inform the volume necessary to seed 1,000,000 cells in each dish. After 24 hours (Day 1), it was confirmed that the cells adhered to the dish, indicating the cells were viable. Upon viability confirmation, cells received the planned light treatment. Treatments were repeated on Days 2 and 3. Culture media was replaced daily to maintain optimal experimental glucose or mannitol concentrations. As a result, media collected from the plates for experimentation was conditioned with MCs from Day 3 into Day 4 (***Figure 9***).

Light Treatment: The cells were subjected to one 670 nm light treatment with an LED array powered by Quantum Devices SpectraLife (Quantum Devices Inc. Barneveld, WI) per day for three days at the daily dosage of 4.5 J/cm^2 (0.025 W/cm^2) for 180 seconds (***Fig 10B***). Treatments were administered by placing dishes directly on the light as demonstrated in ***Fig 10A***. Each light treated group had a sham counterpart that was cultured under identical conditions save exposure to the LED array (***Figure 10C***). One day after the final light treatment, cultured media was collected, and cells were counted and pelleted; both sample types were stored at -80°C until sample processing. Evaluation of PBM efficacy post-hyperglycemic insult represents DR patients that have likely experienced years of fluctuating glucose levels. Despite close maintenance of blood sugar, repeated dysregulation of endocrine homeostasis is expected to be retained as metabolic memory and influences exacerbated dysfunction.

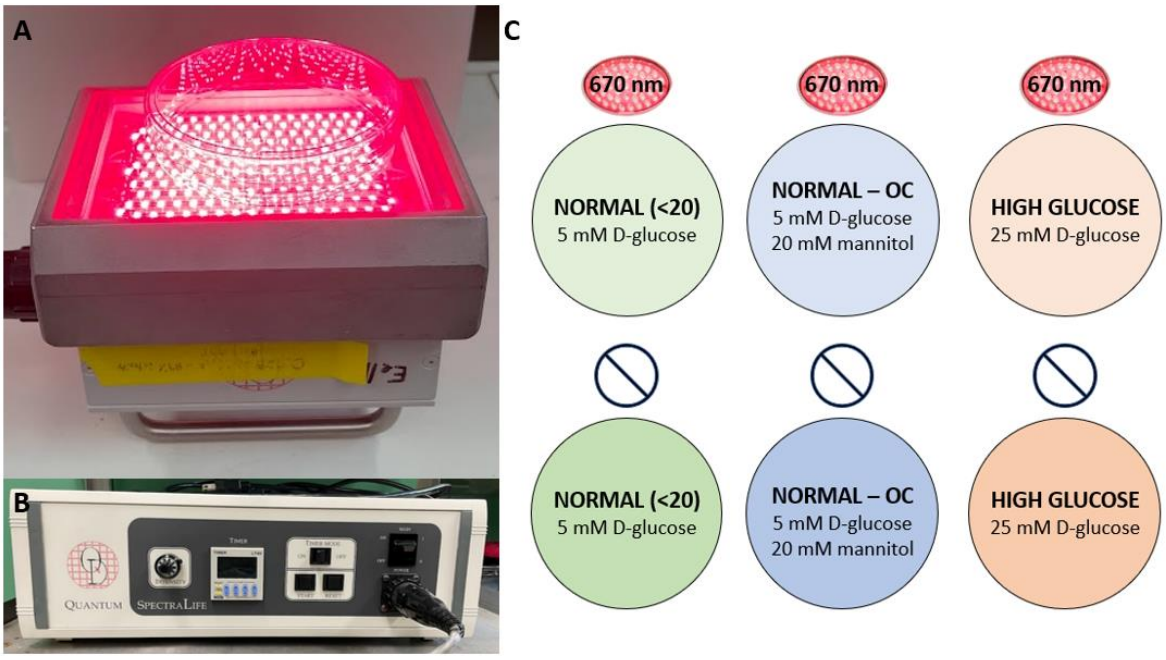

Figure 10: Light treatment setup. *A) Plate positioning during photobiomodulation treatment. B) Light box energy source. C) Representation of six experimental groups; 3 PBM groups, 3 sham groups.*

Sample preparation: Ice cold cell pellets were lysed with radioimmunoprecipitation assay buffer (Sigma R0278). Protein integrity was maintained with the addition of Halt protease inhibitor cocktail (ThermoFisher 78429). Unconcentrated cell lysate samples were used for Western blotting, however, sample concentration with 3 kDa centrifugal filters (Millipore UFC500324) was necessary for multiplexing. Conditioned media required concentration with Amicon Ultra 3 kDa Centrifugal Filters (Millipore UFC800324) for both assays. Unpredicted technical errors forced multiple repetitions of the multiplex assay to obtain successful semi-quantitative measurements. Samples were thawed and refrozen with each repetition leading to concerns about the effect of repeated shocking temperature changes on protein integrity. To restore confidence in the quality of sample, a second batch of conditioned media was concentrated from the unaltered stock prior to the multiplex assay represented in the following text. All concentrated and unconcentrated lysate and media samples were stored at -20°C until analysis. Total protein quantities of each sample were visualized with Coomassie Protein Assay Reagent (ThermoScientific 1856209) and compared to a bovine serum albumin standard curve with the upper and lower detection limits ranging from 2,000 ug/mL to 31.25 ug/mL, respectively. Absorbance values for each sample were examined in duplicate on a 96-well plate reader (BioTek Synergy HT) set at 595 nm to determine average protein concentration.

Western blotting: The basic principle of Western blotting utilized in this investigation relied on separation of proteins via sodium dodecyl sulphate-polyacrylamide gel electrophoresis (SDS-PAGE) followed by electric transfer and detection of target proteins on a stable membrane. SDS is a negatively charged detergent that neutralizes the influence of varied protein charges and

ensures protein separation is based solely on molecular weight. In more words, net positively charged proteins travel through porous gel toward a negatively charge terminal. Small proteins travel rapidly, allowing the distance traveled to exceed that of larger proteins that traverse the gel with more resistance inherent to the gel structure. A ladder with predefined and dye-labeled benchmarks was loaded directly adjacent to samples so molecular weight of unknown proteins could be identified with relative confidence. Both the ladder and proteins were transferred out of the gel and securely bound to a hydrophobic polyvinylidene fluoride (PVDF) membrane by applying a perpendicular electric field. Upon transfer, a blocking agent was introduced to protect areas of the membrane not bound with protein from non-specifically binding antibodies introduced in the next step of the procedure. Primary antibodies specifically bound the proteins of interest, and secondary antibodies conjugated with a detection enzyme specifically bound the primary antibodies. On the day of imaging, membranes were incubated with a reagent that initiates an enzymatic reaction and generated a chemiluminescent profile that could be digitally captured for future analysis.

5X Sample buffer (5 mL glycerol, 2 g SDS, 10 mg bromophenol blue, 6.25 mL 1 M TrisHCl pH 6.8 [final 0.3 M], total volume 20 mL) was added to 50 ug of each lysate (suspended in 1X PBS) and media sample at a 5:1 ratio. 1 M dithiothreitol (DTT) was added at time of use to chemically reduce disulfide bonds (final 100 mM), and proteins were further linearized by boiling for 15 minutes at 95°C before loading into 4-15% polyacrylamide precast gels (Bio Rad 4561084). Precision Plus Kaleidoscope ladder (Bio Rad 1610375) was included on every membrane to visualize the molecular weight range of 10 – 250 kDa and confirm protein presence at the

expected locations for TSP-1 (165 – 198 kDa), GAPDH (37 kDa), and TGF-β (12 [monomer], 25 [dimer], 45 – 65 [latent] kDa) (***Supplementary Figure 1***). Electrophoresis (160 V, 42 minutes) using Mini-PROTEAN Tetra Cell (Bio Rad) separated proteins that were subsequently transferred to PVDF membrane overnight in a cold room (100 mA, 16.65 hours, ~5-9°C) using Mini Trans-Blot Cell (Bio Rad). Successful protein transfer was confirmed by total protein analysis using Swift Membrane Stain (G Biosciences 786-677), as dictated by the product insert. Subsequently, membranes were blocked for 1 hour with 5% milk dissolved in TBST before horizontally bisecting at 75 kDa. The 75 – 250 kDa membrane pieces containing TSP-1 and the 10 – 75 kDa pieces containing GAPDH were separately incubated with their primary antibodies overnight (~5-9°C). Anti-TSP-1 antibody (Santa Cruz Biotechnology sc-59887, 1:200) and anti-GAPDH antibody (Cell Signaling Technology, 1:1,000) were used in combination with Peroxidase AffiniPure Goat Anti-Mouse IgG (Jackson ImmunoResearch Laboratories 111035003, 1:5,000) and Peroxidase AffiniPure Goat Anti-Rabbit IgG (Jackson ImmunoResearch 111035144, 1:10,000), respectively. Three ten-minute washes with 1X TBST eliminated unbound primary antibody. Secondary antibodies were incubated for one hour at room temperature, followed by four washes with 1X TBST and one final wash with 1X TBS. The addition of SuperSignal West Femto Maximum Sensitivity Substrate (ThermoScientific 34094) and SuperSignal West Pico Chemiluminescent Substrate (ThermoScientific 34080) to lysate and media blots, respectively, permitted digital chemiluminescent imaging via ChemiDoc Imaging System (Bio Rad). Chemiluminescent signals obtained via Western blot were normalized to their respective internal loading controls. Lysate blots were normalized to the ubiquitous housekeeping protein GAPDH, but conditioned media blots were normalized to the total protein signal between 100 – 250 kDa as determined by

staining with Swift. This range was selected because densely congregated immunoglobins at 50 – 75 kDa prevented accurate lane separation in quantification software.

Western blot data for cell lysate and conditioned media groups were studied independently. Within-blot variation for lysate and media blots was addressed by normalizing to GAPDH and total protein content, respectively. Between-blot analyses were made possible by normalizing these values to a control, or the normal glucose plus sham (N+Sham) group. Sample quantity limitations prevented loading of this sample on every blot. One out of the four lysate blots lacked N+Sham, but the relationship between N+Sham and high glucose plus sham (HG+Sham) on a separate blot was captured in a ratio and used to normalize these values (***Supplementary Figure 2***; ***Supplementary Table 1***). A similar approach was applied to the conditioned media experiments. Two out of the six blots lacked N+Sham, and a different two out of the six blots contained N+Sham with HG+Sham, or the groups used to create the normalizing ratio. A seven-fold difference between these ratios was observed, so averaging the two numbers generated a third ratio. To avoid bias, the three ratios were individually employed to normalize the necessary blots (***Supplementary Figure 3***; ***Supplementary Table 2***).

Multiplexing: Bead-based assays may be used for detection of protein or nucleic acid. Microbeads or microspheres, autologically named in literature, are microscopic bioreactive granules of robust composition (i.e., metal, glass, silicon, ceramic, polymers) with carboxyl-rooted proteins, nucleic acids, or monoclonal antibodies coating the exterior. The substantial surface area to volume ratio facilitates efficient detection of analytes on a bead's surface. The

term multiplexing in this context refers to the ability to detect multiple analytes in a single assay due to the ability to distinguish between multiple microscopic beads.

The microbead technology used in the present experiments involves magnetic spheres capable of species-specific fluorescent-based detection in the Luminex MAGPIX machine (R&D Systems). Polymer-based polystyrene beads encased a thin layer of magnetite which was necessary to enable solid-state planar bead analysis. Assays were formulated with a set of beads correlated to the selected proteins of interest. Each bead was tagged with multiple copies of a single type of carboxyl-linked detection probe and could be identified by distinct combination of red and near-infrared fluorophores (***Figure 11***).

Figure 11: Structure of xMAP beads

In execution of this assay, target proteins (e.g., inflammation-related cytokines) interacted with microbeads fitted with target-specific ligands. Fluorescent molecules were biotinylated to the ligand/protein complex, and samples were individually assessed in the machine's detection chamber where engaging the magnet locked the beads in a 2D array. Red LED excitation generated a set of fluorescent signals that were captured by the CCD camera wherein the proportion of red and near-infrared fluorescent emission was unique and correlated to the bead identity. Once the beads were identified as one of the four cytokine-related beads, a second phase of signal capture with green LEDs reveals whether the analyte was in fact detected by the beads present in the 2D sampling. Detection data were collected and processed for

interpretation by the software. Protein concentration within a sample could then be determined by referencing a standard curve.

As previously mentioned, both lysate and conditioned media samples required concentration to fall within the analyzable range based on a 1:3 dilution series standard curve. All reagents were prepared according to the kit's instructions on the morning of the assay. The instrument settings were input to reflect 50 uL sample volume, 50 counts per region, and the microparticle regions for each analyte were specific to the Certificates of Analyses.

Statistical Analysis: One-way ANOVA followed by Bonferroni's multiple comparisons test were applied to the western blot data sets. Statistics and graphing for each of the three conditioned media normalizing ratios previously mentioned were completed. Viewing the graphs side-by-side demonstrated that switching between the three normalizing ratios was virtually unimpactful.

RESULTS

Specific Aim 1: Identify expression of anti-angiogenic proteins under high glucose conditions in a cultured Müller cell model of diabetic retinopathy and when treated with 670 nm PBMT. Our working hypothesis was that hyperglycemia would increase expression of these proteins, and 670 nm PBM would further enhance their expression in treated MCs.

Rationale: A non-diseased eye maintains a careful balance between angiogenesis-inducing and angiogenesis-inhibiting growth factors. VEGF is integrally involved in initiating angiogenesis

(Simo, Carrasco, Garcia-Ramirez, & Hernandez, 2006) (Witmer, Vrensen, Van Noorden, & Schlingermann, 2003) and has been the focus of numerous therapeutic DR studies, but previous experiments from Nonorath et al. (2021) did not support VEGF-modification by PBM at 670nm in rMC-1 cells. Therefore, other target proteins require exploration in this context.

Thrombospondin-1 (TSP-1) is an anti-angiogenic extracellular matrix-associated glycoprotein that not only inhibits migration and proliferation of ECs, but also induces EC apoptosis to limit the spread of vascular growth (*Jimenez, et al., 2000)*. Importantly, examination of growth factor ratios and bovine retinal EC responses demonstrated that anti-proliferative activity of the protein was independent of VEGF activity *(Eichler, Yafai, Wiedemann, & Reichenbach, 2004)*. TSP-1 restricts angiogenesis by increasing binding of the transcription factor NF-κB to DNA *(Aurora, et al., 2010)*, which also elevates expression of pro-inflammatory cytokines IL-6, TNF-α, and IL-1β *(Xing, et al., 2017)*. Despite contributing to inflammation, TSP-1 has an immunoregulatory role such that TSP-1-induced apoptosis may eliminate cells that would otherwise continue secreting the aforementioned cytokines. Adequate maintenance of TSP-1 expression is vital to preventing aberrant angiogenesis and progression to DR. Laser photocoagulation, the current primary DR treatment, induces TSP-1 expression *(Binz, et al., 2006)*, so we suspected PBM-induced elevation of this glycoprotein would demonstrate the relevance and potential clinical therapeutic application of light therapy.

Similar to TSP-1, TGF-β is an anti-angiogenic mediator independent of VEGF concentration that inhibits proliferation of ECs *(Eichler, Yafai, Wiedemann, & Reichenbach, 2004)*. TGF-β is secreted

as a multi-component *(Gentry, Lioubin, Purchio, & Marquardt, 1988)* latent protein comprised of a TGF-β dimer and a latent-associated peptide (LAP). The protein complex remains inactive until cleavage of the LAP from the extracellular matrix *(Khan, Joyce, & Tsuda, 2012)*. In addition to being a growth factor, it also functions as an anti-inflammatory cytokine in a number of ways such as influencing induction of aqueous humor Foxp3+RARα+ regulatory T (Treg) cells that promote resolution of inflammation in the otherwise immune-privileged location *(Zhou, Horai, Mattapallil, & Caspi, 2011)*.

Effects of High Glucose on Intracellular and Secreted Thrombospondin-1 in Rat Retinal Müller cells

A. High Glucose Does Not Affect Expression of TSP-1 in Rat Retinal Müller Cells

In planning of this experiment, we intended to have an *n* of 4 with technical duplicates for all substrate and treatment combinations. Unfortunately, unforeseen circumstances forced a two-week delay one day into the western blot protocol for two of the six planned membranes. Limited lysate sample quantities prohibited a repeat experiment to amend the affected *n* number. In total, 2/3 of the lysate sample groups had an *n* of 3, while 1/3 had an *n* of 2 (***Table 1***).

Table 1: N number of cellular lysate and conditioned media groups for western blot experiments

Western Blot – Lysate			
Substrate	*Treatment*	*Sample Label*	*N number*
Normal glucose	PBM	1A	3
Normal glucose	Sham	1B	3
Osmolarity control	PBM	3A	2
Osmolarity control	Sham	3B	3
High glucose	PBM	4A	2
High glucose	Sham	4B	3

Western Blot – Conditioned Media			
Substrate	*Treatment*	*Sample Label*	*N number*
Normal glucose	PBM	1A	4
Normal glucose	Sham	1B	4
Osmolarity control	PBM	3A	4
Osmolarity control	Sham	3B	4
High glucose	PBM	4A	4
High glucose	Sham	4B	4

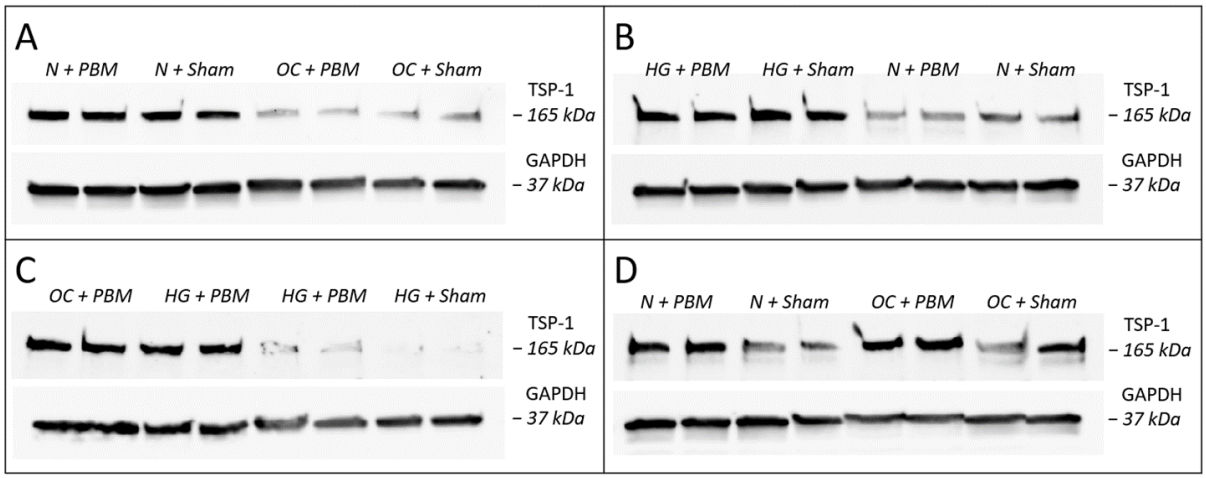

Figure 12: TSP-1 in Muller cell lysate. *Technical duplicates of all samples. Relative protein content determined via western blot. GAPDH bands included for reference. A) Blot 1, B) Blot 2, C) Blot 3, D) Blot 4. Corresponding sample identities noted in* ***Supplementary Table 1****.*

Chemiluminescent bands signaling the presence of TSP-1 were clearly detectable in cellular lysate samples (***Figure 12***). Raw densitometry values are recorded in ***Supplementary Table 3.*** Samples of cells exposed to high glucose adjacent to samples of cells cultured normally only appeared together on one blot (***Fig 13B***), where hyperglycemia appeared to increase TSP-1. In contrast, normalization of blot-to-blot variation indicated that HG did not have an appreciable effect (***Figure 14***).

B. High Glucose Marginally Elevates Extracellular TSP-1 Derived from Rat Retinal Müller Cells

The issue affecting *n* number for the lysate samples was not a concern impacting the conditioned media experiments. Six blots containing technical duplicates for three substrate groups (N, OC, HG) in combination with the two treatment conditions (Sham, PBM) totaled 48-measurements. All planned samples were successfully quantified, resulting in an experimental *n* number of 4 (***Table 1***). Raw densitometry values are listed for reference in ***Supplementary Table 4***.

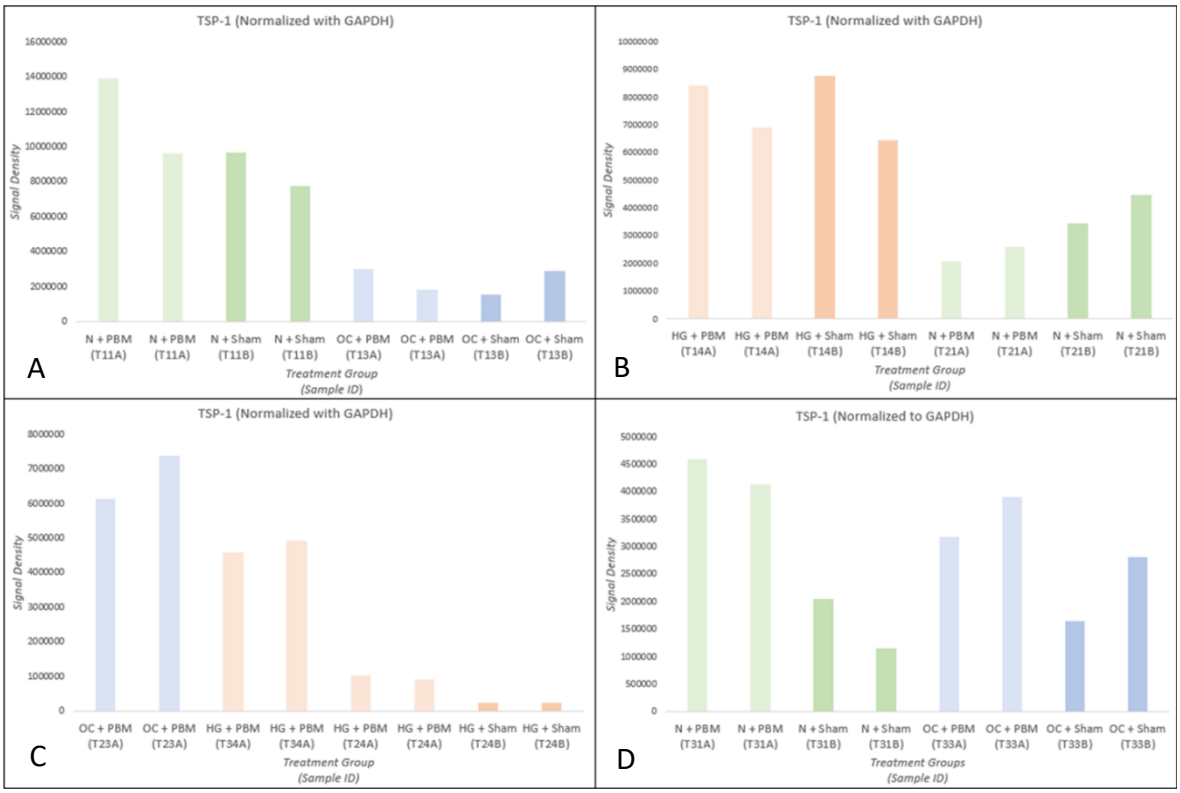

Figure 13: Relative quantity of TSP-1 in Muller cell lysate. *TSP-1 values normalized to GAPDH.*

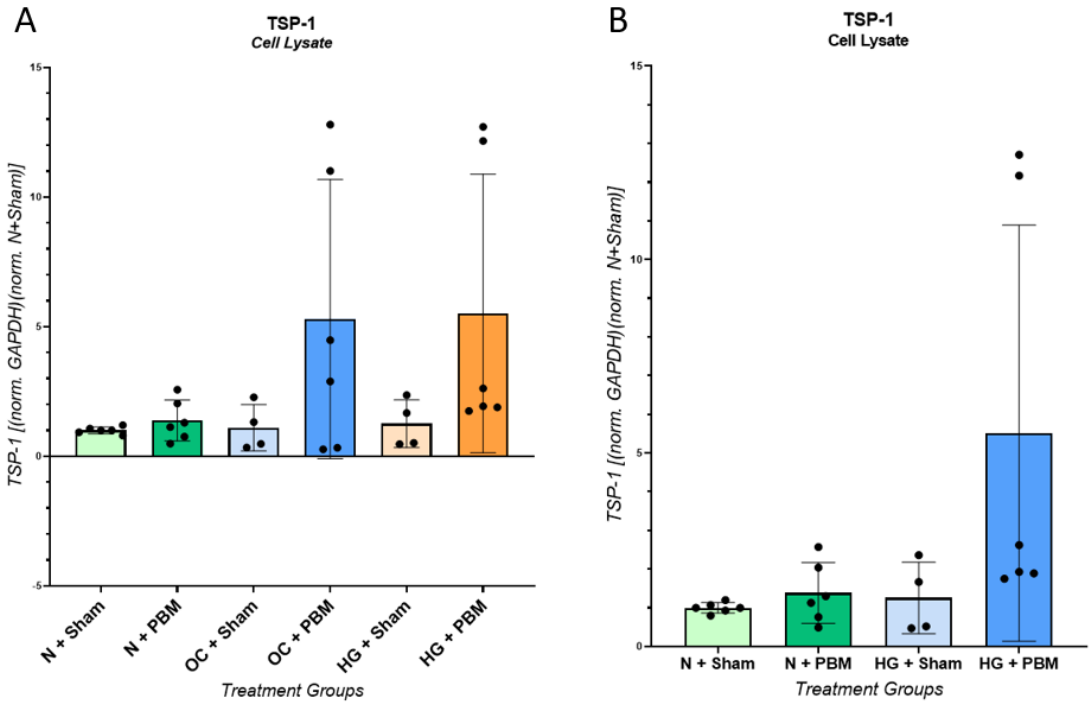

Figure 14: Normalized TSP-1 in Muller cell lysate. *A) Normalized TSP-1 in all three substrate groups (p=0.0702). B) Normalized TSP-1 in normal and high glucose groups (p=0.0463).*

Chemiluminescent bands indicating the presence of TSP-1 were faint and non-specific signal background was raised (***Figure 15***) – specifically blots pictured in ***Fig 15B***, ***Fig 15D***, and ***Fig 15F*** – compared to the intensity and clarity of bands seen in cellular lysate samples (***Figure 12***). When converted to numerical values and plotted, there were noticeable 2- or 3-fold differences between some technical duplicates (***Figure 16***). The largest discrepancy was seen in ***Fig 16A1,*** where there was a 34-fold difference between OC+PBM replicates.

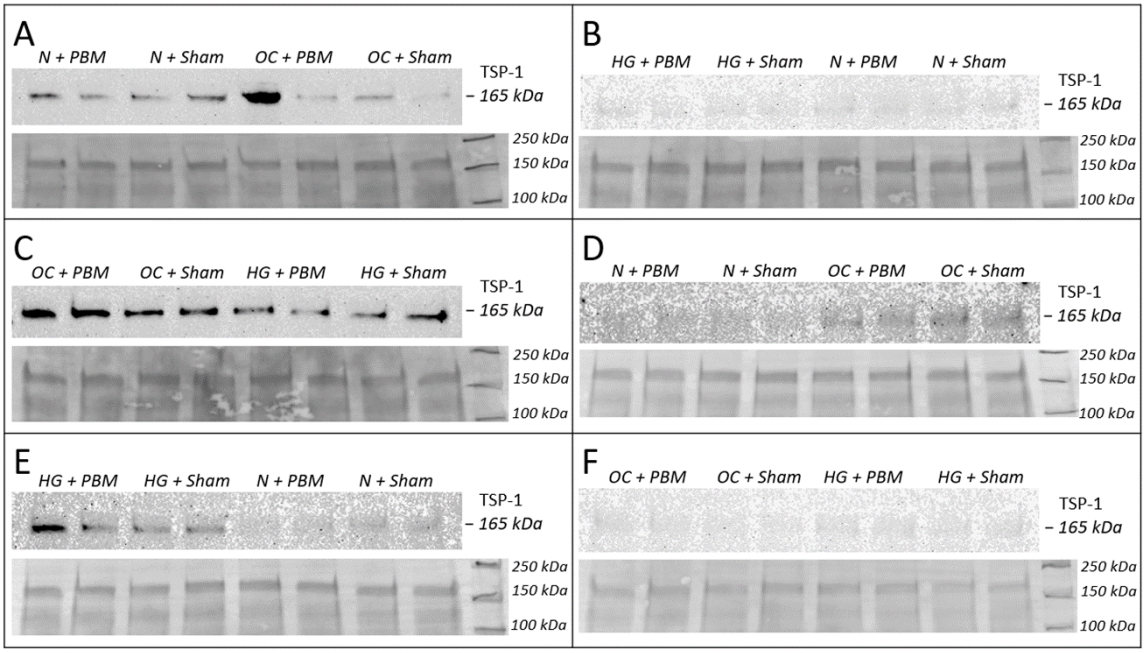

Figure 15: TSP-1 in conditioned media from Muller cells. *Technical duplicates of all samples. Relative protein content determined via western blot. Total protein content between 100 – 250 kDa visualized with Swift stain included as reference. A) Blot 1, B) Blot 2, C) Blot 3, D) Blot 4, E) Blot 5, F) Blot 6.* ***See Supplementary Table 2*** *for sample identities.*

Like the lysate samples, inter-blot media values were normalized prior to drawing final comparisons using the previously defined method. We calculated two N+Sham/HG+Sham ratios, and a third ratio was formed by taking the average. Three normalized datasets were generated (***Supplementary Table 5***) and graphed for comparison (***Figure 17***). The resulting p-values ranged

from 0.3966 – 0.6180 for datasets analyzing all substrate groups (***Fig 17A***, ***Fig 17C***, ***Fig 17E***), and 0.2782 – 0.4532 for datasets excluding osmolarity control (***Fig 17B***, ***Fig 17D***, ***Fig 17F***). Focused comparison of N and HG samples brought the p-values closer to significance ($p < 0.05$), but not nearly enough. Generally, hyperglycemia appeared to induce a minor increase in TSP-1 compared to normal glucose.

Effects of Photobiomodulation on Expression of TSP-1 in Rat Retinal Müller Cells and Culturing Media

A. 670 nm Photobiomodulation Increases Expression of TSP-1 in Müller Glial Cells Under High Glucose Conditions

Figures of normalized data for individual blots depicting relative TSP-1 content suggested that PBM could elevate intracellular protein content (***Figure 13***). All three substrate groups (N, OC, HG) demonstrated a trend of increased TSP-1 in PBM-treated cells in at least one of the experiments (***Fig 13A*** – *N*; ***Fig 13C*** – *HG*; ***Fig 13D*** – *N*; ***Fig 13D*** – *OC*). However, data also supports that PBM does not have a discernible (***Fig 13A*** – *OC*; ***Fig 13B*** – *HG*) or depreciable (***Fig 13B*** – *N*) effect on TSP-1 expression. Although the relative amount of intracellular TSP-1 appeared to vary between the normal glucose and osmolarity control groups, the relationships between sham and PBM within these groups are similar. Between blot variation was addressed via normalization with N+Sham values, or the equalizing N+Sham/HG+Sham ratio previously described. ***Figure 14A*** represents the amount of TSP-1 detected in each of the three substrate groups. No significant differences between any group means were detected ($p = 0.0702$), however, TSP-1 tended to be

elevated in groups treated with PBM if not supplemented with normal levels of glucose. Statistical analysis was conducted a second time after eliminating the mannitol PBM and sham groups to focus on the N and HG data, and the alternate p-value did signify the existence of a meaningful difference between means ($p = 0.0463$) (***Fig 14B***). Despite this, the individual groups were not found to be significantly different.

B. 670 nm Photobiomodulation Increases Expression of TSP-1 in Hyperglycemic Media Cultured with Müller Glial Cells

Figure 17 shows the results of six different normalization calculations. Numerical values are listed in ***Supplementary Table 5***. N+Sham and N+PBM values are noticeably unaffected by interchanging the normalizing ratio despite manipulated OC and HG values. This is explained by the distribution of samples between blots. N+Sham and N+PBM were not on any blot normalized with the ratios because the presence of N+Sham negated the need for its application. All ratio variations indicate that the light treatment did not affect secretion of TSP-1 in the normal concentration of glucose (***Figure 17***). Contrastingly, most calculations show a trend of elevated TSP-1 in PBM-treated rMC-1 cells. Despite the perceived trend, the graph closest to displaying significance between group means still broadly missed the mark ($p \not< 0.05$; $p = 0.2782$) (***Figure 17B***).

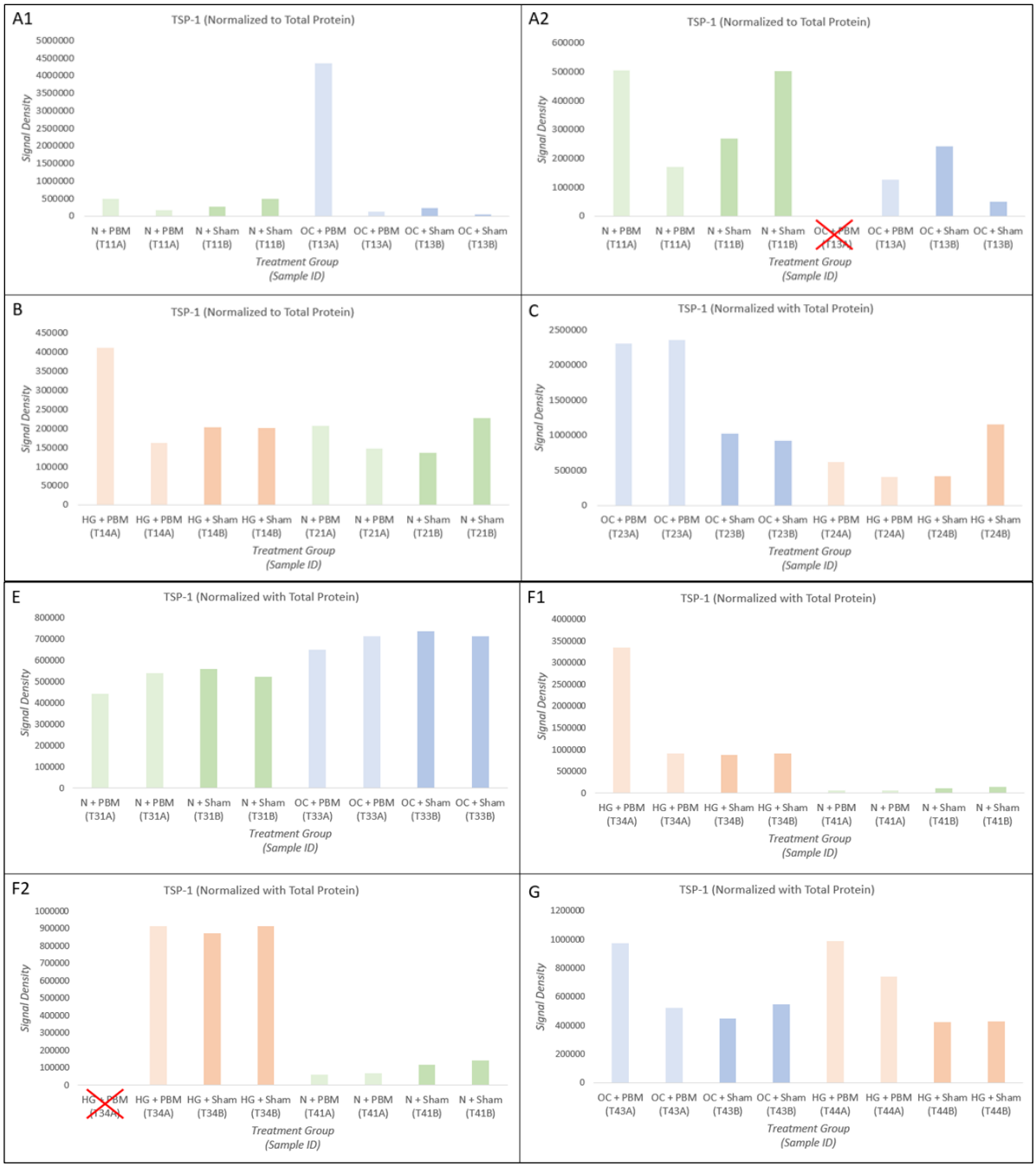

Figure 16: Relative quantity of TSP-1 in Muller cell conditioned media*. TSP-1 values normalized to total protein. A1 and A2 represent identical information, excluding lane 5. E1 and E2 represent identical information, excluding lane 1. Visual outliers in A1 and E1 eliminated in A2 and E2 to improve scale of remaining measurements.*

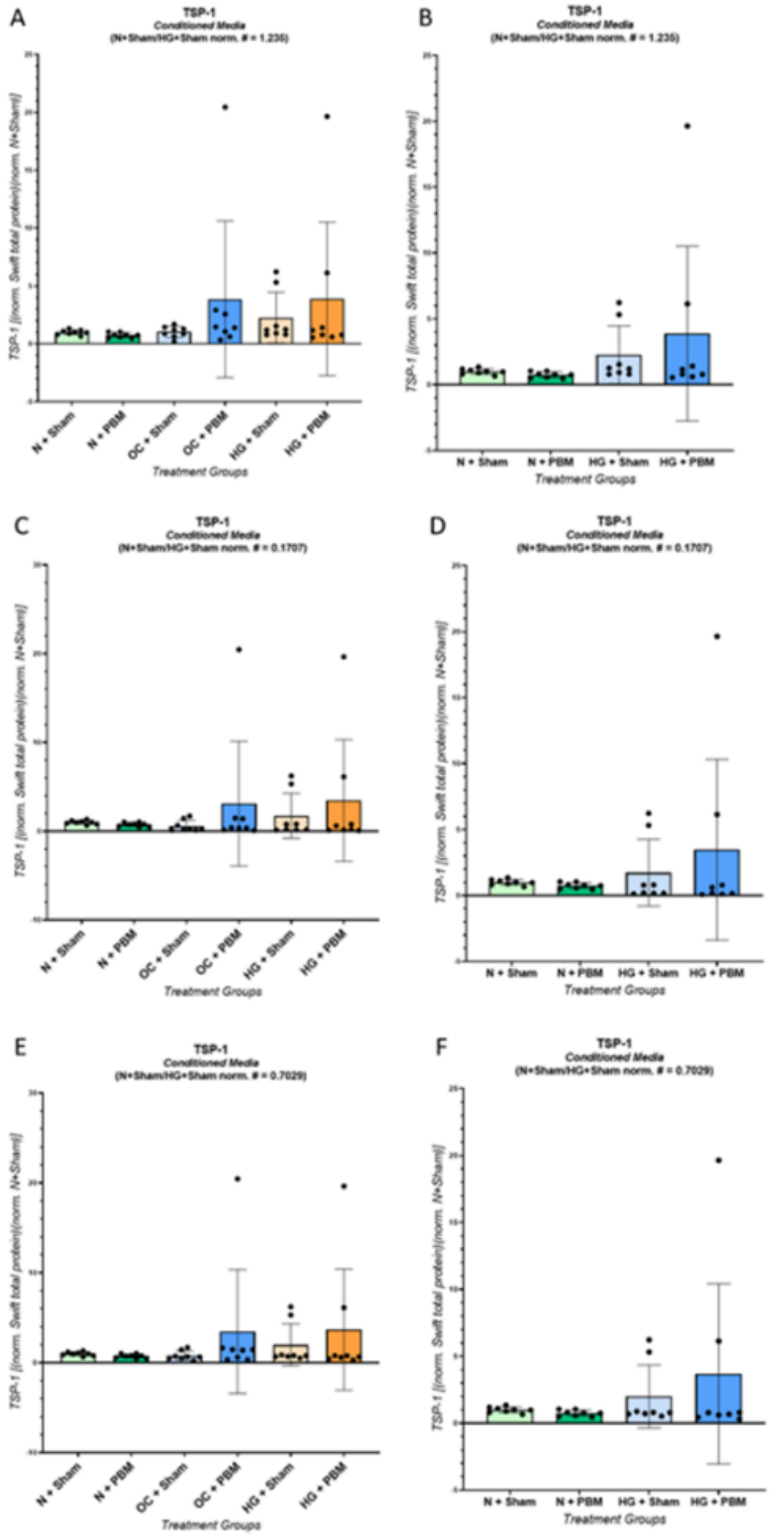

Fig 17: Normalized TSP-1 in Muller cell conditioned media. *A) Normalized TSP-1 in all three substrate groups (p = 0.3966), and B) Normalized TSP-1 in normal and high glucose groups (p = 0.2782) using N+Sham/HG+Sham ratio 1.235. C) Normalized TSP-1 in all three substrate groups (p = 0.6180), and D) Normalized TSP-1 in normal and high glucose groups (p = 0.4532) using N+Sham/HG+Sham ratio 0.1707. E) Normalized TSP-1 in all three substrate groups (p = 0.5086), and F) Normalized TSP-1 in normal and high glucose groups (p = 0.3626) using N+Sham/HG+Sham ratio 0.7029.*

Effect of 670 nm Photobiomodulation on TGF-β Expression Remains Unelucidated Due to Serum Interference

Initially, we planned to analyze TGF-β expression via ELISA since this type of assay has a greater quantitative capacity than Western blotting. This method was decided against because isolation and quantification of active versus inactive TGF-β is challenging to accomplish. Western blotting was selected because the three protein forms could be clearly differentiated based on molecular weight and we would be able to achieve a near equivalent goal.

Several weeks were dedicated to optimizing Western blotting conditions for detection of TGF-β (Cell Signaling Technology 3711); however, we struggled to isolate a scientifically valuable chemiluminescent signal for this protein. The primary antibody selected for TGF-β asserts to detect all three isoforms of recombinant TGF-β in addition to endogenous levels of TGF-β1 precursor proteins. Protein bands at the expected monomer, dimer, and latent (dimer + LAP) locations (12, 25, 45-65 kDa, respectively) consistently displayed oversaturated chemiluminescent signals even at low total protein loading volumes and dilute primary and secondary antibody concentrations (***Figure 18***).

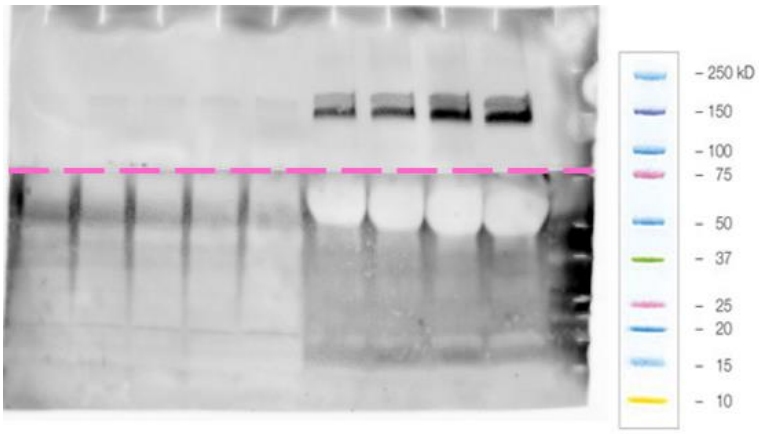

Figure 18: Serum interference with visualization of TGF-β. *Membrane cut at 75 kDa so pieces could be blotted independently. Reconstruction of membrane pieces post-imaging juxtaposes clarity of TSP-1 bands (top) to oversaturated chemiluminescence of TGF-β (bottom).*

Specific Aim 2: Identify inflammatory and angiogeneic cytokines expressed under high glucose conditions in a cultured Müller cell model of diabetic retinopathy and determine the effect of 670 nm PBMT. Our working hypothesis was that high glucose will increase expression of inflammatory cytokines, but light therapy at 670 nm would cause a subsequent reduction.

Rationale: Many pro-inflammatory cytokines also enhance angiogenesis either directly to induce EC growth or indirectly accomplish the same objective by inducing secretion of angiogenic mediators. A study from Gerhardinger et al. (2005) found that 26 of 78 assessed genes upregulated in STZ-diabetic rats were associated with the inflammatory response, including a precursor NF-κB subunit, p105. Activation and nuclear translocation of the transcription factor NF-κB can result in expression of proinflammatory cytokines including IL-1β, IL-6 and TNF-α; however, subsequent qPCR analysis by the researchers only supported significant upregulation of IL-1β in the diabetic rat retina *(Gerhardinger, et al., 2005)* (***Figure 19***). While some studies like

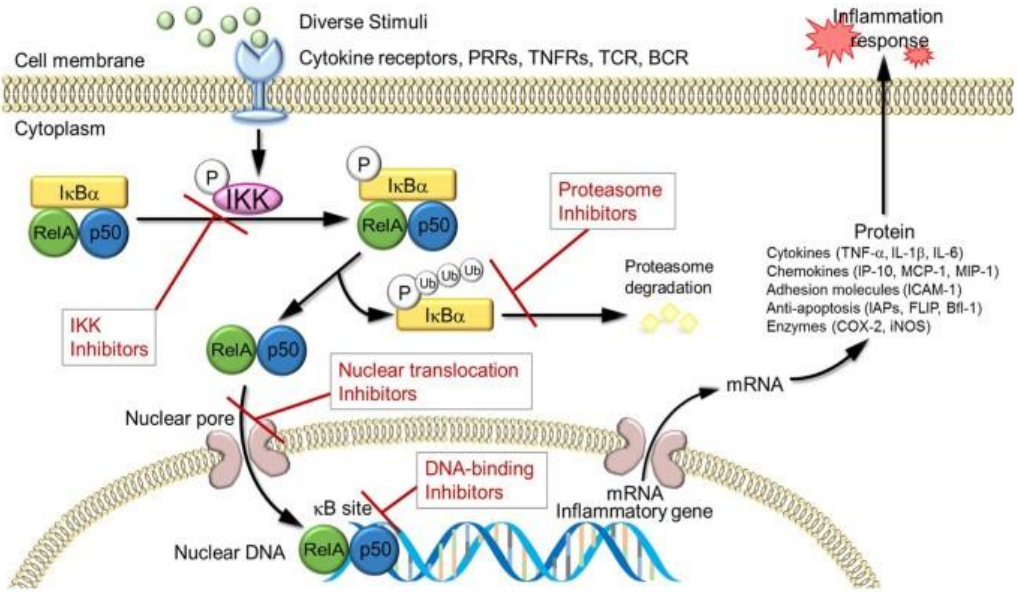

Figure 19: NF-κB signaling pathway *(Liu, Zhang, Joo, & Sun, 2017)*

this evaluate the pre-translational mRNA transcripts, other studies take it one step farther and approach analysis of cytokine expression by quantifying the actual post-translational proteins. Importantly, both types of analyses generate valuable data for scientific interpretation. Researchers have largely found elevated expression of inflammatory cytokines in blood serum and the eye in patients and DR models when compared to controls (***Supplemental Table 6***). Hyperglycemic inflammation segues into further expression of proteins that become destructive mechanisms when unregulated as can be seen in ***Figure 20***.

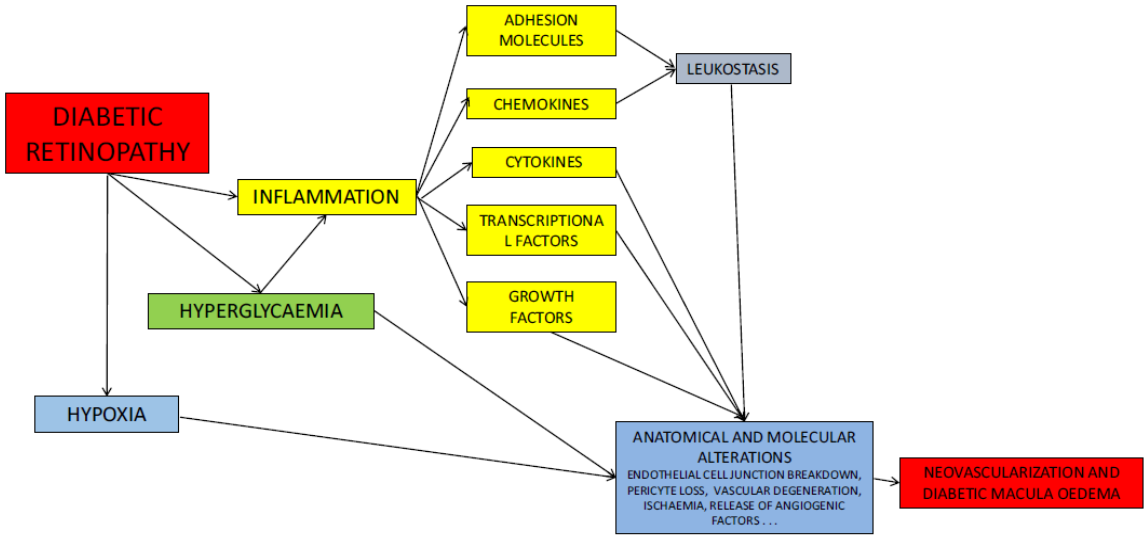

Figure 20: The pathogenesis of diabetic retinopathy *(Semeraro, et al., 2019)*

Effects of High Glucose and Photobiomodulation on Expression of Inflammation-Associated Proteins in Rat Retinal Müller Cells Remains Untested

Unfortunately, results of hyperglycemia and modifications due to PBM could not be identified for intracellular inflammatory protein expression. Consecutive complications with the Luminex

instrument resulted in lost sample and insufficient amounts of cellular lysate necessary to continue running informative assays.

Effects of High Glucose and Photobiomodulation on Secretion of Inflammation-Associated Proteins Secreted by Rat Retinal Müller Cells Could Not Be Established at the Measured Concentrations

The 96-well assay plate accommodated three technical replicates for each sample (***Supplementary Figure 6***). Previous experimentation with the kit suggested that dilution of samples 1:1, 1:5, and 1:10 would broaden the range of detection so that measurements at most dilutions would fall within the standard curves for each analyte. The multiplex kit provided a six-point standard curve diluted 1:3, but we continued the dilution series and extended the curves to eight points in an effort to enhance the lower range of detection. After the assay, mean fluorescence intensities (MFI) of the protein standards were evaluated for adherence to the dilution pattern. The average fluorescence seen in standards 6, 7, and 8 was often comparable instead of following the anticipated 1:3 dilution trend. Moreso, examination of the unknown sample MFI data for each of the four proteins (***Tables 2 – 5***) and the respective standard curves (***Figures 21 – 24***) revealed that none of the inflammation-related proteins fell in the only range of relative quantitative confidence between standards 1 and 5. Few experimental standard curves adhere precisely to the calculated dilutions, but the inability to distinguish between standards 6 through 8 made unknown samples with MFIs within that muddied range particularly unreliable. Consequently, the concentrations of IL-1β, IL-6, TNF-α, and IL-10 could not be calculated due to the assay sensitivity.

Table 2: MFI for IL-1β in media conditioned with Muller cells					
Treatment	**Sample**	**1:1 dil. MFI**	**1:5 dil. MFI**	**1:10 dil. MFI**	**Avg MFI**
N + Sham	T11B	13	13	12	12.67
N + Sham	T21B	12	12	11	11.67
N + Sham	T31B	11	11	11	11.00
N + Sham	T41B	12	11	11	11.33
N + PBM	T11A	12	13	13	12.67
N + PBM	T21A	12	12	12	12.00
N + PBM	T31A	10	11	11	10.67
N + PBM	T41A	12	11	11	11.33
OC + Sham	T13B	13	13	11	12.33
OC + Sham	T23B	11	12	11	11.33
OC + Sham	T33B	12	11	11	11.33
OC + Sham	T43B	11	11	11	11.00
OC + PBM	T13A	12	13	12	12.33
OC + PBM	T23A	11	11	12	11.33
OC + PBM	T33A	11	24	11	15.33
OC + PBM	T43A	11	11	10	10.67
HG + Sham	T14B	13	13	12	12.67
HG + Sham	T24B	11	12	11	11.33
HG + Sham	T34B	11	10	11	10.67
HG + Sham	T44B	11	11	11	11.00
HG + PBM	T14A	13	12	12	12.33
HG + PBM	T24A	11	11	11	11.00
HG + PBM	T34A	11	11	11	11.00
HG + PBM	T44A	11	11	11	11.00

Table 3: MFI for IL-6 in media conditioned with Muller cells					
Treatment	**Sample**	**1:1 dil. MFI**	**1:5 dil. MFI**	**1:10 dil. MFI**	**Avg MFI**
N + Sham	T11B	42	42	41	41.67
N + Sham	T21B	40	41	40	40.33
N + Sham	T31B	NaN	37	38	37.50
N + Sham	T41B	41	41	40	40.67
N + PBM	T11A	43	42	41	42.00
N + PBM	T21A	40	41	40	40.33
N + PBM	T31A	40	39	38	39.00
N + PBM	T41A	40	41	38	39.67
OC + Sham	T13B	43	41	39	41.00
OC + Sham	T23B	40	41	41	40.67
OC + Sham	T33B	45	40	41	42.00
OC + Sham	T43B	45	38	41	41.33
OC + PBM	T13A	42	40	41	41.00
OC + PBM	T23A	39	38	40	39.00
OC + PBM	T33A	41	55	38	44.67
OC + PBM	T43A	45	38	39	40.67
HG + Sham	T14B	41	42	41	41.33
HG + Sham	T24B	40	41	40	40.33
HG + Sham	T34B	39	39	40	39.33
HG + Sham	T44B	41	39	40	40.00
HG + PBM	T14A	43	40	40	41.00
HG + PBM	T24A	42	39.5	41	40.83
HG + PBM	T34A	41.5	40	38	39.83
HG + PBM	T44A	40	40	39	39.67

Standards	*Replicate 1*	*Replicate 2*	*Avg MFI*
Standard 1	2617.5	2603.5	2610.5
Standard 2	1047.5	1151	1099.25
Standard 3	349	398.5	373.75
Standard 4	130	138	134
Standard 5	51	50	50.5
Standard 6	25	26	25.5
Standard 7	16	16	16
Standard 8	14	13	13.5

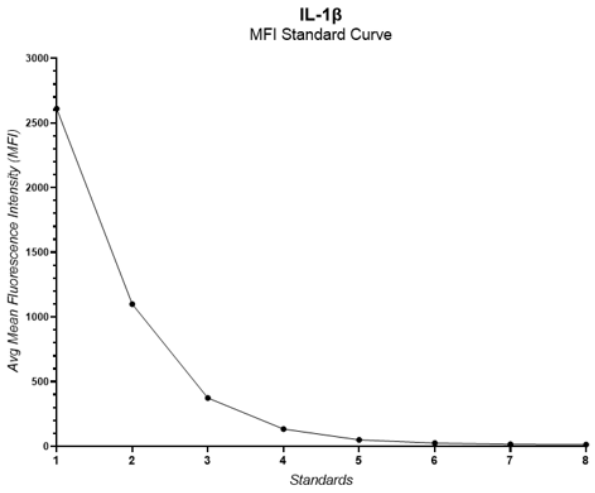

Figure 21: Standard curve MFI for IL-1β in media conditioned with Muller cells

Standards	*Replicate 1*	*Replicate 2*	*Avg MFI*
Standard 1	2149	2165.5	2157.25
Standard 2	1051	1145.5	1098.25
Standard 3	466	513	489.5
Standard 4	207	221	214
Standard 5	97	98	97.5
Standard 6	58	62	60
Standard 7	47	47	47
Standard 8	43	42	42.5

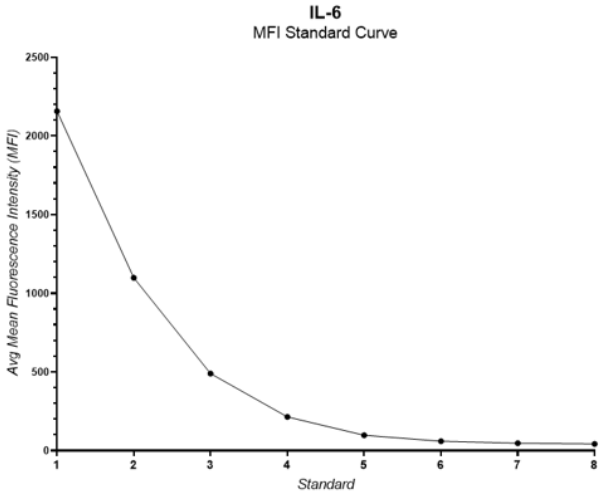

Figure 22: Standard curve MFI for IL-6 in media conditioned with Muller cells

Table 4: MFI for TNF-α in media conditioned with Muller cells					
Treatment	*Sample*	*1:1 dil. MFI*	*1:5 dil. MFI*	*1:10 dil. MFI*	*Avg MFI*
N + Sham	T11B	20	20	20	20.00
N + Sham	T21B	19	19	19	19.00
N + Sham	T31B	17	18	18	17.67
N + Sham	T41B	18	18	18	18.00
N + PBM	T11A	19.5	20	19	19.50
N + PBM	T21A	20	19	19.5	19.50
N + PBM	T31A	17	18	18	17.67
N + PBM	T41A	18	18	17	17.67
OC + Sham	T13B	20	20	18	19.33
OC + Sham	T23B	18	19	18	18.33
OC + Sham	T33B	18	19	19	18.67
OC + Sham	T43B	18	17	18	17.67
OC + PBM	T13A	19	20	19	19.33
OC + PBM	T23A	17	18	18	17.67
OC + PBM	T33A	18	31	18	22.33
OC + PBM	T43A	18	17	17	17.33
HG + Sham	T14B	19	20	19	19.33
HG + Sham	T24B	17	18	18	17.67
HG + Sham	T34B	18	17	17	17.33
HG + Sham	T44B	18	17	17	17.33
HG + PBM	T14A	20	19	19	19.33
HG + PBM	T24A	18	17	18	17.67
HG + PBM	T34A	17	18	17	17.33
HG + PBM	T44A	18	18	18	18.00

Table 5: MFI for IL-10 in media conditioned with Muller cells					
Treatment	*Sample*	*1:1 dil. MFI*	*1:5 dil. MFI*	*1:10 dil. MFI*	*Avg MFI*
N + Sham	T11B	31	33	33	32.33
N + Sham	T21B	31	32	30	31.00
N + Sham	T31B	27	29	28	28.00
N + Sham	T41B	30.5	29	29	29.50
N + PBM	T11A	32	33	32	32.33
N + PBM	T21A	31	31	32	31.33
N + PBM	T31A	29	30	28	29.00
N + PBM	T41A	28	30	27	28.33
OC + Sham	T13B	34	33	30	32.33
OC + Sham	T23B	30	32	30.5	30.83
OC + Sham	T33B	31	29	30	30.00
OC + Sham	T43B	29	28	28	28.33
OC + PBM	T13A	33	33	31.5	32.50
OC + PBM	T23A	27	29	31	29.00
OC + PBM	T33A	28	42	29	33.00
OC + PBM	T43A	28	28	28	28.00
HG + Sham	T14B	32	33	32	32.33
HG + Sham	T24B	27	31	31	29.67
HG + Sham	T34B	29	28	29	28.67
HG + Sham	T44B	29	28	28.5	28.50
HG + PBM	T14A	33	31	31	31.67
HG + PBM	T24A	29	29	30	29.33
HG + PBM	T34A	29	28	28	28.33
HG + PBM	T44A	30	28	28	28.67

Standards	*Replicate 1*	*Replicate 2*	*Avg MFI*
Standard 1	2116	2140	2128
Standard 2	1164.5	1267	1215.75
Standard 3	511	572	541.5
Standard 4	215	232	223.5
Standard 5	88	88.5	88.25
Standard 6	42	44	43
Standard 7	27	27	27
Standard 8	22	22	22

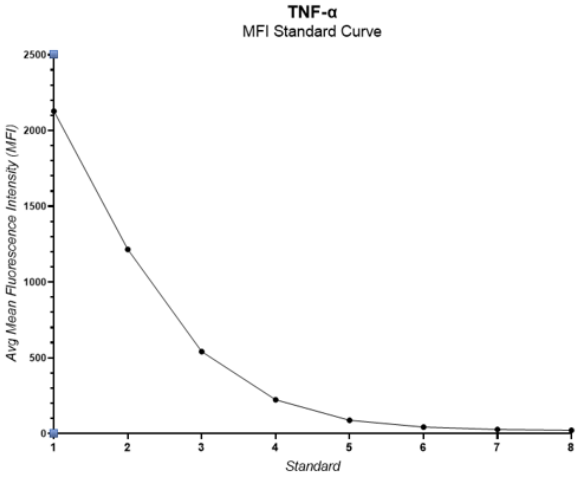

Figure 23: Standard curve MFI for TNF-α in media conditioned with Muller cells

Standards	Replicate 1	Replicate 2	Avg MFI
Standard 1	1948	1999	1973.5
Standard 2	748	833.5	790.75
Standard 3	266	304	285
Standard 4	115	123	119
Standard 5	60	59	59.5
Standard 6	42	42	42
Standard 7	36	35	35.5
Standard 8	34	32	33

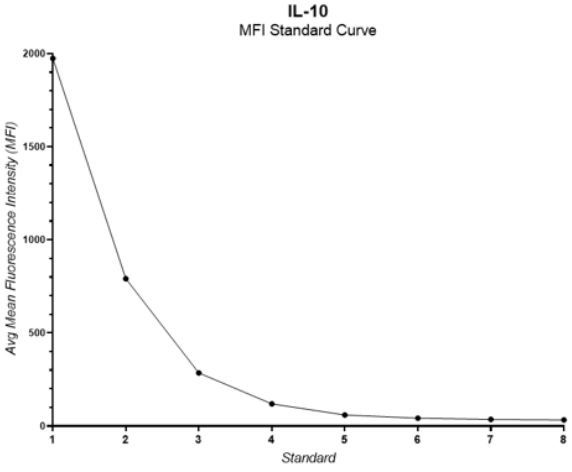

Figure 24: Standard curve MFI for IL-10 in media conditioned with Muller cells

DISCUSSION

In this study, we asked two related questions in an attempt to further the field of diabetic retinopathy research. 'How does hyperglycemia affect the expression of angiogenic and inflammatory proteins in MCs', and, 'does 670 nm PBM alter the expression of these proteins?' Western blot and multiplexing assays facilitated relative quantification of angiogenic, and inflammatory proteins believed to be linked to DR pathogenesis.

Our findings suggest that hyperglycemia does not have a significant impact on the amount of intracellular or extracellular TSP-1 derived from rat retinal MCs. High glucose appeared to mildly elevate contribution to secreted TSP-1, but within the cell, TSP-1 levels remained unaffected. As hypothesized, incorporating light therapy tended to increase TSP-1 production in cells subjected to glycemic distress, but this finding lacked significance ($p<0.05$). Additionally, we were unable to visualize TGF-β due to serum interference. Likewise, unanticipated assay sensitivity limitations prevented quantification of IL-1β, IL-6, IL-10, and TNF-α in Müller cell conditioned media as sample concentration measurements failed to fall within the standard curves.

MCs have been found to secrete TSP-1 under normal conditions to sustain an angiostatic environment, but expression significantly increases under cellular distress (i.e., hypoxia) (*Yafai, et al., 2014) (Eichler, Yafai, Wiedemann, & Reichenbach, 2004)*. It has been shown that TSP-1 expression is elevated in diabetic murine hearts *(Wahab, et al., 2005)*, vasculature *(Wahab, et al., 2005)*, and human kidneys *(Wahab, et al., 2005)*; the same may not be true in diabetic eyes according to an exploratory study from Wang et al. (2009). Vitreous fluid was collected from

diabetic and non-diabetic patients during vitrectomies for Western blot analysis. ImageJ software allowed the researchers to semi-quantitatively compare band intensity, and it was revealed that TSP-1 levels were consistently lower and wider ranging in diabetic patients versus the age-matched controls *(Wang, Gottlieb, Sorenson, & Sheibani, 2009)*. This reflects the expected loss of anti-angiogenic mediators and consequent vasculopathy in DR patients. Angiogenesis-inhibiting proteins like TSP-1 are necessary to ensure cells maintain a functional and non-pathogenic balance of vessel growth.

DM increases TGF-β expression in the retinal vasculature. This alteration was demonstrated to enhance stability of newly formed vessels and confer protection from ischemia and, consequently, further angiogenesis *(Dagher, et al., 2017)*. There are three established mammalian isoforms of this protein, but TGF-β1 and more so TGF-β2 are the predominant isoforms found in the eye *(Eastlake, et al., 2016)*. Eichler et al. (2004) compared the anti-proliferative capacity of TSP-1, TGF-β2, and pigment epithelium-derived factor (PEDF), another anti-angiogenic factor, and concluded that TGF-β2 inhibited proliferation of bovine retinal ECs most effectively. Thus, increasing expression of this protein and its less abundant counterpart, TGF-β1, via PBM could have significant implications for vascular control in DR patients.

In the present study, TGF-β chemiluminescent signals obtained via Western blot appeared oversaturated. Investigation into what may have caused this issue revealed that 10% FBS has been documented to contain between 1,000 and 2,000 pg/ml of latent TGF-β *(Oida & Weiner, 2010) (Danielpour, et al., 1989)*. If we speculate that a similar ratio of TGF-β is present in 2% FBS

as was used to culture Müller cells in our experiments, 200 to 400 pg/mL of the protein quantified could be expected to originate from the FBS alone. Although the previous studies examined the presence of latent TGF-beta, the signal was also oversaturated for the monomer and dimer expected locations.

The intended method to analyze expression of TGF-β in hyperglycemic and/or light treated rat retinal Müller cells was western blotting. Future research aiming to successfully quantify this protein through cell culture should limit the addition of FBS to culture medium when possible. Latent TGF-β is known to be present in FBS, so quantifying TGF-β derived from the cell model alone requires its elimination to prevent interfering with the intended measurement. Since a primary purpose of adding FBS to media is enhancement of nutrient content and promotion of cell growth, eliminating this component affects cell viability. Serum interference prevented quantification of TGF-β with the selected method, so we researched our options moving forward. We concluded we could: 1) identify an assay where FBS would not skew analyte quantification, or 2) repeat cell culturing and light treatment experiments in the absence of FBS. The first option was decidedly not financially feasible because western blotting was chosen partially for its affordability since few items required purchasing to complete the project. The second option was also rejected not only due to time limitations, but also due to the lab's historical struggle to generate viable MC in a serum-free environment. Although challenging, it is possible to maintain immortal cells in an FBS-free environment, so one approach might be to cultivate cells with FBS media until immediately prior to the treatment and collection of samples.

Western blotting has persisted in research for decades, but the technique refrained from becoming obsolete as other protein quantification technologies entered the market. We selected chemiluminescent detection because it is an appropriate first step in observing the relationship between nutritional source and potential treatments. Results from these assays are semi-quantitative and, in some instances, variable. The fold change between the highest and lowest duplicate averages on individual lysate blots was between 3-fold and 5-fold for all but one blot. The fourth blot showed a 52-fold change between the highest duplicate average (OC + PBM) and the lowest (HG + Sham) (***Figure 13C***). They are different substrate and treatment groups, indeed, yet the results don't match what one would expect based on the similarity between the groups in the other three blots. One explanation traces back to unexplained membrane damage on the relevant blot, an issue illuminated by the total protein staining process. A second stain attempt was imaged and revealed the same pattern of deterioration, suggesting a problem with the PVDF membrane, and not the imaging technique (***Figure 25***). In the process of quantification and normalization, damage affecting discreteness of GAPDH bands (**Fig 12C**) and clarity of Swift stain between 100 and 250 kDa (**Fig 15C**) likely affected the calculations.

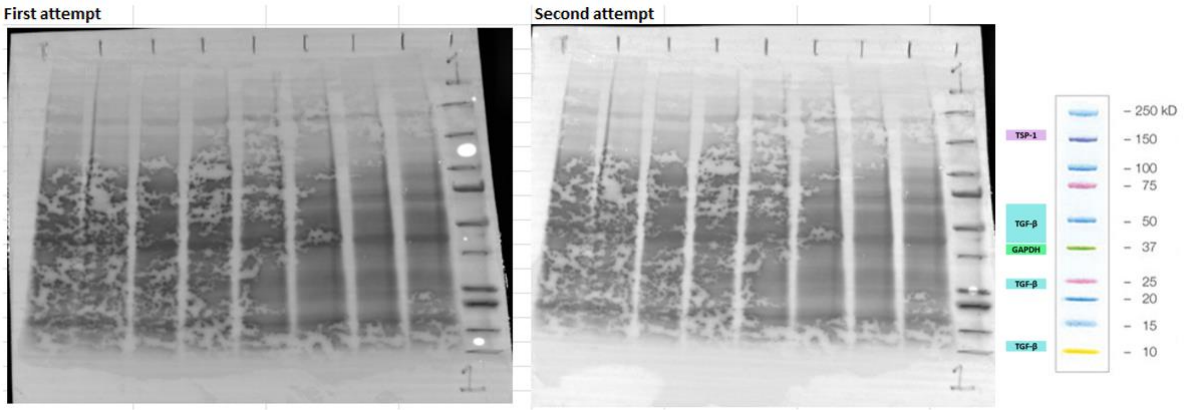

Figure 25: Membrane damage to third lysate blot (L3).

Another observation of inconsistency is the contrast between one HG + PBM sample and its duplicate in ***Figure 16A1***. This visually unusual value is surprising because of the stark irregularity with its technical replicate. The chemiluminescent signal in lane 6 was over 30-fold greater than its lane 5 counterpart. Reinvestigation of the total protein quantities in these lanes revealed the protein content was virtually identical and did not clarify this discrepancy.

Some inconsistencies were wholly unexpected. Mannitol was selected as the substrate to supplement media to provide osmotic pressure without raising the glycemic index based on its use in related diabetes experiments. If a true control, results of this group would resemble the group unchallenged with high glucose. Interestingly, TSP-1 levels in the OC+Sham group resembled the HG+Sham group stronger than the N+Sham group (***Figure 14***). The mannitol-supplemented group may not have behaved as anticipated for any combination of two reasons. First, mannose as a sugar molecule structurally and metabolically differs from glucose. It's possible that this substrate in the experiments influenced secondary protein processing via glycosylation, somehow modifying the rate of TSP-1 biosynthesis. Other D-glucose alternative exist, so this theory could be explored by replacing mannitol with 3-methyl-*o*-glucose, L-glucose, or dextran. The other potential reason is that elevated osmolarity alone induced a cellular alteration. A study based in bovine retinal endothelial cells reported correlation between high osmolarity from any source and increased NO and superoxide *(El-Remessy, Abou-Mohamed, Caldwell, & Caldwell, 2003)*; ***Figure 3*** demonstrates the involvement of these molecules with inflammatory signaling and eventual cellular dysfunction. Regrettably, it's not possible to

completely eliminate the stress of elevated osmotic pressure regardless of incorporation of a non-glycemic substitute.

While intensity of the TGF-β signal was consistently oversaturated, we encountered the opposite problem in our pursuit to quantify proteins involved in inflammation. Fluorescence indicative of IL-1β, IL-6, IL-10, and TNF-α presence was consistently on the low end of the standard curve. This suggested that the kit used lacked the sensitivity necessary to distinguish reliable measurements. All conditioned media samples were concentrated prior to the assay and one of the three replicates was entirely undiluted, yet the values could not be guided into quantifiable range. The Luminex Discovery Assay protocol detailed a 6-point standard curve, but we continued the 1:3 dilution twice to increase it to 8-points. We intended this extension to elevate assay sensitivity, but this failed for every analyte as evidenced by the similarity in MFI between standards 6, 7, and 8. Luminex also provided expected standard curve concentration ranges for all proteins, so one could deduce that the protein content in the media is close to or less than the low end of the range (***Table 6***). This raises the question of whether protein content in these samples is generally low, or whether it is these proteins specifically that are so sparsely distributed.

Rat Premixed Multi-analyte Kit
Luminex Discovery Assay

Analyte	*Standard Curve (pg/mL)*
IL-1β	18.5 – 4,500
IL-6	170 – 4,300
TNF-α	232 – 56,400
IL-10	19.7 – 4,790

Table 6: Standard curve for analytes in Rat Premixed Multi-analyte Kit LXSARM

As Müller cells are structurally integrated in the retina, studies assessing retinal cytokine expression in DR patients would have been ideal to formulate initial hypotheses. Collection of retinal samples from living patients is invasive and unrealistic; therefore, retinal protein expression can only be evaluated in diabetic models (***Supplementary Table 6***). When diabetes was induced with streptozotocin in rodents, retinal IL-1β *(Kowluru & Odenbach, 2004) (Vincent & Mohr, 2007)* and TNF-α *(Joussen, et al., 2002)* mRNA were significantly elevated. As an alternative to measurements obtained directly from human retinal samples, we can rely on data from ocular fluids (e.g., vitreous, and aqueous humor) collected from willing patients during ophthalmic procedures. In these studies, DR patients often demonstrated elevated IL-β *(Wu, Hwang, Song, & Tao, 2017) (Patel, Saleh, Hykin, Gregor, & Cree, 2008) (Demircan, Safran, Soylu, Ozcan, & Sizmaz, 2006) (Tsai, et al., 2018) (Mao & Yan, 2014)*, IL-6 *(Wu, Hwang, Song, & Tao, 2017) (Chen, Zhang, Liao, & Wen, 2017) (Yuuki, et al., 2001)*, TNF-α *(Wu, Hwang, Song, & Tao, 2017) (Demircan, Safran, Soylu, Ozcan, & Sizmaz, 2006) (McAuley, et al., 2014)*, and IL-10 *(Wu, Hwang, Song, & Tao, 2017) (Mao & Yan, 2014) (Tan, Zou, Yoshida, Jiang, & Zhou, 2020)*. Other studies have found these cytokine levels to be unchanged between diseased and control groups *(Chen, Zhang, Liao, & Wen, 2017) (Loporchio, et al., 2021) (Tsai, et al., 2018) (Yuuki, et al., 2001)*, but no studies could be found with data suggesting a decrease in the inflammatory markers. Altogether, these findings support that the DR disease state is characteristically inflamed. Our findings were not able to contribute to the quantifying context like the discussed studies. IL-1β, IL-6, IL-10, and TNF-α were not found to exist in sufficient quantities for detection even in the HG groups which is where we had hypothesized an elevation. That is not to say that HG does not

induce a change, rather, we were not able to gather reliable data points to contextualize the relationship between protein expression between normal and hyperglycemic cells.

IL-1β is infamously classified as a pro-inflammatory cytokine, but it remains an inactive pro-cytokine until specialized cell receptors detect pathogen- or danger-associated molecular patterns and activate the NLRP3 inflammasome and caspase signaling cascade. Activated IL-1β interacts with surface-expressed IL-1R1 and communicates the presence of threat *(Dinarello, 2018)*. The result of IL-1β signaling is well-characterized and multi-fold in that numerous biological outcomes have been documented. Not only can IL-1β exacerbate inflammation in immortalized human MCs (MIO-M1) by inducing expression of IL-8, IL-6, and additional IL-1β in a suggested autocrine feedback loop *(Liu, et al., 2014) (Yoshida, Sotozono, Ikeda, & Kinoshita, 2001)*, but also the cytokine contributes to vascular permeability, angiogenesis, and leukostasis in other cultured cell lines *(Essani, et al., 1998) (Wyble, et al., 1997)*.

Like IL-1β, the secreted cytokines IL-6 and TNF-α, are labeled pro-angiogenic and pro-inflammatory. IL-6 induces VEGF *(Ye & Steinle, 2017) (Cohen, Nahari, Cerem, Neufeld, & Levi, 1996)* and matrix metalloproteinases (MMPs) *(Legendre, Bogdanowicz, Boumediene, & Pujol, 2005) (Symeonidis, et al., 2011)* for vascular remodeling, while TNF-α encourages leukostasis and intensified inflammation through induction of adhesion molecules *(Wyble, et al., 1997)*, IL-6 *(Yoshida, Sotozono, Ikeda, & Kinoshita, 2001)*, and IL-8 *(Liu, et al., 2014)*. When unchecked, each of these mechanisms may result in harmful regional modifications including breakdown of the BRB *(Luna, et al., 1997)*, degeneration and acellularization of retinal capillaries *(Kowluru &*

Odenbach, 2004) (Zheng, Howell, Hatala, Huang, & Kern, 2007), and prolonged activation of microglia leading to a pathogenic state known as gliosis *(Grigsby, et al., 2014) (Fletcher, Phipps, & Wilkinson-Berka, 2005)*. Though measured inflammation is beneficial to enact protective host mechanisms, anti-inflammatory cytokines like IL-10 are essential to maintain balance of aberrant activity.

Interestingly, IL-1β, IL-6, and TNF-α production was found to correlate TSP-1 expression via the NF-κB pathway in a human monocytic cell line stimulated to induce inflammatory conditions *(Xing, et al., 2017)*, further demonstrating the interconnected nature of the inflammatory and angiogenic signaling pathways. Since VEGF does not appear to be modified by PBM *(Nonorath, et al., 2021)*, perhaps attenuation of the inducing proteins in this study will lead to reduced VEGF over a longer duration than has been evaluated in previous studies.

Photobiomodulation, like any therapeutic, requires ample optimization to identify best practices in inducing ideal modifications to a system to restore homeostasis. One study involving DM patients without a DR diagnosis saw a decrease in macular and retinal thickness paired with improved vision *(Ramin, Ahadi, & Ebrahimi, 2021)*. A different study explored another transitional phase in disease progression. DR patients without DME received light therapy resulting in reduced macular thickness and decelerated progression of the disease *(Tang, Herda, & Kern, 2014)*. Studies should continue to edit the temporal distribution of light treatments to optimize procurement of intended results. If results in the aforementioned studies are trusted, preventative PBM may be viable to implement before the disease state can be fully realized. All

things considered, the diversity of variables involved in formulating educated treatment decisions for a vison threatening disease present in epidemic proportions should continue to be investigated.

FUTURE DIRECTIONS AND CONCLUSION

The number of Americans diagnosed with diabetic retinopathy is projected to reach nearly 15 million by the year 2030 *(Diabetic Retinopathy Data and Statistics, 2020)*, and a void of available treatments often leaves medical professionals in a position unequip to aid patients beyond moderate symptom management. This study examined the effects of high glucose with and in absence of a 670nm light treatment regimen in rat retinal Müller cells.

Any number of modifications could be made to the above experiments to explore new hypotheses related to the pathogenesis and potential treatments of DR. Immortalized rat Müller cells (rMC-1) have been identified as a suitable DR model and thus were used in this project *(Tang, et al., 2013) (Nonorath, et al., 2021)*. The disadvantage of immortalized cell lines is the lack of exposure to the complete biological system. This study demonstrates that MCs produce important angiogenic and inflammatory mediators suspected of contributing to the dysfunction suffered by vascular ECs. Coculturing ECs with MCs, potentially with knockouts of the relevant proteins, would immerse cells into a more realistic model that could elucidate the cellular interplay preceding vascular dysfunction. Utilization of primary cells is an alternative way to incorporate the influence of external variables on systemic dysfunction. Participation in the anatomical area of interest surrounded by the dynamic molecular milieu until the moment of harvest has its advantages in acquiring results reflective of the larger organism. Trends in protein

expression seen in immortalized cells may not be matched in primary cells exposed to identical glucose and PBM conditions and could further inspire inquisitions to determine the source of the inconsistency. Animal models continue to have a significant role in biomedical research; controlling for genetics, environmental conditions, and other variables considered to be unethical in human research is a privilege that cannot be overlooked. While grateful for animal models as an irreplaceable step in establishing initial observations, testing potential treatments on human cells should be an eventual goal. Substituting rMC-1 cells with immortalized human MCs (MIO-M1) or primary ocular tissues harvested postmortem in the above experiments would further the ability to translate treatments between species. In addition to modification of the disease model, future studies may find value in altering the cellular culturing conditions. The mannitol group was intended to control for osmotic pressure differences between the normal and high glucose groups, but the unexpected dissimilarity to the normal group in western blotting suggests a potential change in the cell metabolism. Dextran, 3-methyl-o-glucose, or L-glucose may be a more suitable substrate to function as a control for osmolarity. As the field of light therapy advances, theories regarding the optimal wavelength, intensity, or duration of treatment may shift. Accordingly, informed alterations to the presented experiments could be applied. In general, preventing disease manifestation is favored to treating downstream ailments, so preconditioning cells with PBM prior to a hyperglycemic assault could expand on the viability of this option.

Science is productive in that there is educational value in all experimentation. A scientists' pursuit for answers involves analyzing existing work from peers, evaluating best practices in the field,

and developing a methodology to test hypotheses based on available resources and tools. Throughout the study, multiple attempts to acquire data were unsuccessful and experiments required repetition until an adequate dataset could be collected. The colloquialism ‘Hindsight is 20/20’ aptly describes one’s outlook in the wake of a seemingly failed experiment. The twice awarded Nobel Prize laureate Marie Curie is quoted addressing the circuitous nature of research: “I was taught that the way of progress was neither swift nor easy.” Nevertheless, a true scientist will resolve feelings of discouragement with renewed enthusiasm to answer the questions that feed the flame of enlightenment.

REFERENCES

Aiello, L. P., Avery, R. L., Arrigg, P. G., Keyt, B. A., Jampel, H. D., Shah, S. T., . . . Park, J. E. (1994). Vascular endothelial growth factor in ocular fluid of patients with diabetic retinopathy and other retinal disorders. *N Engl J Med, 331*(22), 1480-1487. doi:10.1056/NEJM199412013312203

Anderzen, J., Samuelsson, U., Gudbjornsdottir, S., Hanberger, L., & Akesson, K. (2016). Teenagers with poor metabolic control already have a higher risk of microvascular complications as young adults. *J Diabetes Complications, 30*(3), 533-536. doi:10.1016/j.jdiacomp.2015.12.004

Antonetti, D. A., Klein, R., & Gardner, T. W. (2012). Diabetic retinopathy. *N Engl J Med, 366*(13), 1227-1239. doi:10.1056/NEJMra1005073

Ao, J., Wood, J. P., Chidlow, G., Gillies, M. C., & Casson, R. J. (2018). Retinal pigment epithelium in the pathogenesis of age-related macular degeneration and photobiomodulation as a potential therapy? *Clin Exp Ophthalmol, 46*(6), 670-686. doi:10.1111/ceo.13121

Ao, J., Wood, J. P., Chidlow, G., Gillies, M. C., & Casson, R. J. (2018). Retinal pigment epithelium in the pathogenesis of age-related macular degeneration and photobiomodulation as a potential therapy? *Clin Exp Ophthalmol, 46*(6), 670-686. doi: 10.1111/ceo.13121

Aurora, A. B., Biyashev, D., Mirochnik, Y., Zaichuk, T. A., Sanchez-Martinez, C., Renault, M.-A., . . . Volpert, O. V. (2010). NF-kappaB balances vascular regression and angiogenesis via chromatin remodeling and NFAT displacement. *Blood, 116*(3), 475-484. doi:10.1182/blood-2009-07-232132

Berka, J. L., Stubbs, A. J., Wang, D. Z., DiNicolantonio, R., Alcorn, D., Campbell, D. J., & Skinner, S. L. (1995). Renin-containing Müller cells of the retina display endocrine features. *Invest Ophthalmol Vis Sci, 36*(7), 1450-1458.

Binz, N., Graham, C. E., Simpson, K., Lai, Y. K., Shen, W.-Y., Lai, C.-M., . . . Rakoczy, P. E. (2006). Long-term effect of therapeutic laser photocoagulation on gene expression in the eye. *FASEB J, 20*(2), 383-385. doi:10.1096/fj.05-3890fje

Bringmann, A., Pannicke, T., Grosche, J., Francke, M., Wiedemann, P., Skatchkov, S. N., . . . Reichenbach, A. (2006). Müller cells in the healthy and diseased retina. *Prog Retin Eye Res, 25*(4), 397-424. doi:10.1016/j.preteyeres.2006.05.003

Brownlee, M. (2005). A lucid discussion of the molecular pathways involved in the development of diabetic microvascular complications. *Diabetes, 54*, 1615-1625.

Busik, J. V., Mohr, S., & Grant, M. B. (2008). Hyperglycemia-induced reactive oxygen species toxicity to endothelial cells is dependent on paracrine mediators. *Diabetes, 57*(7), 1952-1965. doi:10.2337/db07-1520

Busik, J. V., Mohr, S., & Grant, M. B. (2008). Hyperglycemia-induced reactive oxygen species toxicity to endothelial cells is dependent on paracrine mediators. *Diabetes, 57*(7), 1952-1965. doi:10.2337/db07-1520

Centers for Disease Control and Prevention. (2020). *National Diabetes Statistics Report, 2020.* Atlanta, GA: Centers for Disease Control and Prevention, U.S. Dept of Health and Human Services.

Chen, H., Zhang, X., Liao, N., & Wen, F. (2017). Assessment of biomarkers using multiplex assays in aqueous humor of patients with diabetic retinopathy. *BMC Ophthalmol, 17*(1), 176. doi:0.1186/s12886-017-0572-6

Cohen, T., Nahari, D., Cerem, L. W., Neufeld, G., & Levi, B. Z. (1996). Interleukin 6 induces the expression of vascular endothelial growth factor. *J Biol Chem, 271*(2), 736-741. doi:10.1074/jbc.271.2.736

Coorey, N. J., Shen, W., Chung, S. H., Zhu, L., & Gillies, M. C. (2012). The role of glia in retinal vascular disease. *Clin Exp Optom, 95*(3), 266-281. doi:10.1111/j.1444-0938.2012.00741.x

Crawford, S. E., Stellmach, V., Murphy-Ullrich, J. E., Ribeiro, S. M., Lawler, J., Hynes, R. O., . . . Bouck, N. (1998). Thrombospondin-1 is a major activator of TGF-beta1 in vivo. *Cell, 93*(7), 1159-1170. doi:10.1016/s0092-8674(00)81460-9

Dagher, Z., Gerhardinger, C., Vaz, J., Goodridge, M., Tecilazich, F., & Lorenzi, M. (2017). The increased transforming growth factor-beta signaling induced by diabetes protects retinal vessels. *Am J Pathol, 187*(3), 627-638. doi:10.1016/j.ajpath.2016.11.007

Danielpour, D., Kim, K. Y., Dart, L. L., Watanabe, S., Roberts, A. B., & Sporn, M. B. (1989). Sandwich enzyme-linked immunosorbent assays (SELISAs) quantitate and distinguish two forms of transforming growth factor-beta (TGF-beta 1 and TGF-beta 2) in complex biological fluids. *Growth Factors, 2*(1), 61-71. doi:10.3109/08977198909069082

De La Cadena, R. A., Rico, M. C., Del Carpio-Cano, F., Safadi, F., Kunapuli, S. P., Smith, G., . . . Igbre, A. (2011). Thrombospondin-1 (TSP1), Transforming Growth Factor-Beta (TGFb) and Connective Tissue Growth Factor (CTGF) are Involved in the Pathophysiology of Diabetic Retinopathy. *Blood*. doi:10.1182/blood.V118.21.3275.3275

Demircan, N., Safran, B. G., Soylu, M., Ozcan, A. A., & Sizmaz, S. (2006). Determination of vitreous interleukin-1 (IL-1) and tumour necrosis factor (TNF) levels in proliferative diabetic retinopathy. *Eye (Lond), 20*(12), 1366-1369. doi:10.1038/sj.eye.6702138

Diabetic Retinopathy Data and Statistics. (2020, November 19). Retrieved 2022, from National Eye Institute: https://www.nei.nih.gov/learn-about-eye-health/outreach-campaigns-and-resources/eye-health-data-and-statistics/diabetic-retinopathy-data-and-statistics

Dinarello, C. A. (2018). Overview of the IL-1 family in innate inflammation and acquired immunity. *Immunol Rev, 281*(1), 8-27. doi:10.1111/imr.12621

Eastlake, K., Banerjee, P. J., Angbohang, A., Charteris, D. G., Khaw, P. T., & Limb, G. A. (2016). Müller glia as an important source of cytokines and inflammatory factors present in the gliotic retina during proliferative vitreoretinopathy. *Glia, 64*(4), 495-506. doi:10.1002/glia.22942

Eden, B., & Klein, K. (2007). Overview of epidemiologic studies of diabetic retinopathy. *Ophthalmic Epidemiol, 14*(4), 179-183. doi:10.1080/09286580701396720

Eichler, W., Yafai, Y., Wiedemann, P., & Reichenbach, A. (2004). Angiogenesis-related factors derived from retinal glial (Müller) cells in hypoxia. *Neuroreport, 15*(10), 1633-1637. doi:10.1097/01.wnr.0000133071.00786.a4

El-Remessy, A. B., Abou-Mohamed, G., Caldwell, R. W., & Caldwell, R. B. (2003). High glucose-induced tyrosine nitration in endothelial cells: role of eNOS uncoupling and aldose reductase activation. *Invest Ophthalmol Vis Sci, 44*(7), 3135-3143. doi:10.1167/iovs.02-1022

Essani, N. A., Fisher, M. A., Simmons, C. A., Hoover, J. L., Farhood, A., & Jaeschke, H. (1998). Increased P-selectin gene expression in the liver vasculature and its role in the pathophysiology of neutrophil-induced liver injury in murine endotoxin shock. *J Leuk Biol, 63*(3), 288-296. doi:10.1002/jlb.63.3.288

Feenstra, D. J., Yego, E. C., & Mohr, S. (2013). Modes of retinal cell death in diabetic retinopathy. *J Clin Exp Ophthalmol, 4*(5), 298. doi:10.4172/2155-9570.1000298

Fletcher, E. L., Phipps, J. A., & Wilkinson-Berka, J. L. (2005). Dysfunction of retinal neurons and glia during diabetes. *Clin Exp Optom, 88*(3), 132-145. doi:10.1111/j.1444-0938.2005.tb06686.x

Gentry, L. E., Lioubin, M. N., Purchio, A. F., & Marquardt, H. (1988). Molecular events in the processing of recombinant type 1 pre-protransforming growth factor beta to the mature polypeptide. *Mol Cell Biol, 8*, 4162-4168.

Gerhardinger, C., Costa, M. B., Coulombe, M. C., Toth, I., Hoehn, T., & Grosu, P. (2005). Expression of acute-phase response proteins in retinal Müller cells in diabetes. *Invest Ophthalmol Vis Sci, 46*(1), 349-357. doi:10.1167/iovs.04-0860

Goke, B. (2008). Islet cell function: alpha and beta cells -- partners towards normoglycaemia. *Int J Clin Pract Suppl, 159*, 2-7. doi:10.1111/j.1742-1241.2007.01686.x

Gonzalez-Quesada, C., Cavalera, M., Biernacka, A., Kong, P., Lee, D.-W., Saxena, A., . . . Shinde, A. (2013). Thrombospondin-1 induction in the diabetic myocardium stabilizes the cardiac matrix in addition to promoting vascular rarefaction through angiopoietin-2 upregulation. *Circ Res, 113*(12), 1331-1344. doi:10.1161/CIRCRESAHA.113.302593

Graham, C. E., Binz, N., Shen, W. Y., Constable, I. J., & Rakoczy, E. P. (2006). Laser photocoagulation: ocular research and therapy in diabetic retinopathy. *Adv Exp Med Biol, 572*, 195-200. doi:10.1007/0-387-32442-9_29

Grigsby, J. G., Cardona, S. M., Pouw, C. E., Muniz, A., Mendiola, A. S., Tsin, A. T., . . . Cardona, A. E. (2014). The role of microglia in diabetic retinopathy. *J Ophthalmol, 2014*, 705783. doi:10.1155/2014/705783

Heintz, E., Wirehn, A.-B., Bourghardt Peebo, B., Rosenqvist, U., & Levin, L.-A. (2010). Prevalence and healthcare costs of diabetic retinopathy: a population-based register study in Sweden. *Diabetologia, 53*(10), 2147-2154. doi:10.1007/s00125-010-1836-3

Hosoki, A., Oku, H., Horie, T., Kida, T., Sugiyama, T., Nakamura, K., & Ikeda, T. (2015). Changes in expression of Nestin, CD44, vascular endothelial growth factor, and glutamine synthetase by mature Müller cells after dedifferentiation. *J Ocul Pharmacol Ther, 31*(8), 476-481. doi:10.1089/jop.2014.0117

Hosoya, K.-I., & Tomi, M. (2005). Advances in the cell biology of transport via the inner blood-retinal barrier: establishment of cell lines and transport functions. *Biol Pharm Bull, 28*(1), 1-8. doi:10.1248/bpb.28.1

Irikura, V. M., Lagraoui, M., & Hirsh, D. (2002). The epistatic interrelationships of IL-1, IL-1 receptor antagonist, and the type I IL-1 receptor. *J Immunol, 169*(1), 393-398. doi:10.4049/jimmunol.169.1.393

Jimenez, B., Volpert, O. V., Crawford, S. E., Febbraio, M., Silverstein, R. L., & Bouck, N. (2000). Signals leading to apoptosis-dependent inhibition of neovascularization by thrombospondin-1. *Nat Med, 6*(1), 41-48. doi:10.1038/71517

Joussen, A. M., Poulaki, V., Mitsiades, N., Kirchhof, B., Koizumi, K., Dohmen, S., & Adamis, A. P. (2002). Nonsteroidal anti-inflammatory drugs prevent early diabetic retinopathy via TNF-alpha suppression. *FASEB J, 16*(3), 438-440. doi:10.1096/fj.01-0707fje

Karu, T. (1999). Primary and secondary mechanisms of action of visible to near-IR radiation on cells. *J Photochem Photobiol B, 49*(1), 1-17. doi:10.1016/S1011-1344(98)00219-X

Karu, T. I., & Kolyakov, S. F. (2005). Exact action spectra for cellular responses relevant to phototherapy. *Photomed Laser Surg, 23*, 355-361.

Khan, S. A., Joyce, J., & Tsuda, T. (2012). Quantification of active and total transforming growth factor-β levels in serum and solid organ tissues by bioassay. *BMC Res Notes, 5*, 636. doi:10.1186/1756-0500-5-636

Klein, R., Klein, B. E., & Moss, S. E. (1989). The Wisconsin epidemiological study of diabetic retinopathy: a review. *Diabetes Metab Rev, 5*(7), 559-570. doi:10.1002/dmr.5610050703

Kohn, A. D., Summers, S. A., Birnbaum, M. J., & Roth, R. A. (1996). Expression of a constitutively active Akt Ser/Thr kinase in 3T3-L1 adipocytes stimulates glucose uptake and glucose transporter 4 translocation. *J Biol Chem, 271*(49), 31372-31378. doi:10.1074/jbc.271.49.31372

Komatsu, M., Takei, M., Ishii, H., & Sato, Y. (2013). Glucose-stimulated insulin secretion: A newer perspective. *J Diabetes Investig, 4*(6), 511-516. doi:10.1111/jdi.12094

Kowluru, R. A., & Odenbach, S. (2004). Role of interleukin-1beta in the development of retinopathy in rats: effect of antioxidants. *Invest Ophthalmol Vis Sci, 45*(11), 4161-4166. doi:10.1167/iovs.04-0633

Lane, N. (2006). Cell biology: power games. *Nature, 443*(7114), 901-903. doi:10.1038/443901a

Legendre, F., Bogdanowicz, P., Boumediene, K., & Pujol, J.-P. (2005). Role of interleukin 6 (IL-6)/IL-6R-induced signal tranducers and activators of transcription and mitogen-activated protein kinase/extracellular. *J Rheumatol, 32*(7), 1307-1316.

Li, X., Liu, J., Hoh, J., & Liu, J. (2019). Müller cells in pathological retinal angiogenesis. *Transl Res, 207*, 96-106. doi:10.1016/j.trsl.2018.12.006

Liu, T., Zhang, L., Joo, D., & Sun, S.-C. (2017). NF-κB signaling in inflammation. *Signal Transduct Target Ther, 2*, 17023. doi:10.1038/sigtrans.2017.23

Liu, X., Ye, F., Xiong, H., Hu, D., Limb, G. A., Xie, T., . . . Zhang, D. Y. (2014). IL-1β upregulates IL-8 production in human Müller cells through activation of the p38 MAPK and ERK1/2 signaling pathways. *Inflammation, 37*(5), 1486-1495. doi:10.1007/s10753-014-9874-5

Loporchio, D. F., Tam, E. K., Cho, J., Chung, J., Jun, G. R., Xia, W., . . . Subramanian, M. L. (2021). Cytokine Levels in Human Vitreous in Proliferative Diabetic Retinopathy. *Cells, 10*(5), 1069. doi:10.3390/cells10051069

Luna, J. D., Chan, C. C., Derevjanik, N. L., Mahlow, J., Chiu, C., Peng, B., . . . Vinores, S. A. (1997). Blood-retinal barrier (BRB) breakdown in experimental autoimmune uveoretinitis: comparison with vascular endothelial growth factor, tumor necrosis factor alpha, and interleukin-1beta-mediated breakdown. *J Neurosci Res, 49*(3), 268-280. doi:10.1002/(sici)1097-4547(19970801)49:3<268::aid-jnr2>3.0.co;2-a

Mao, C., & Yan, H. (2014). Roles of elevated intravitreal IL-1β and IL-10 levels in proliferative diabetic retinopathy. *Roles of elevated intravitreal IL-1β and IL-10 levels in proliferative diabetic retinopathy, 62*(6), 699-701. doi:10.4103/0301-4738.136220

McAuley, A. K., Sanfilippo, P. G., Hewitt, A. W., Liang, H., Lamoureux, E., Wang, J. J., & Connell, P. P. (2014). Vitreous biomarkers in diabetic retinopathy: a systematic review and meta-analysis. *J Diabetes Complications, 28*(3), 419-425. doi:10.1016/j.jdiacomp.2013.09.010

Nonorath, H. J., Hall, A. E., SenthiKumar, G., Abroe, B., Eells, J. T., & Liedhegner, E. S. (2021). 670nm photobiomodulation modulates bioenergetics and oxidative stress, in rat Müller cells challenged with high glucose. *PLoS One, 16*(12), e0260968. doi:10.1371/journal.pone.0260968

Oida, T., & Weiner, H. L. (2010). Depletion of TGF-beta from fetal bovine serum. *J Immunol Methods, 362*(1-2), 195-198. doi:10.1016/j.jim.2010.09.008

Patel, J. I., Saleh, G. M., Hykin, P. G., Gregor, Z. J., & Cree, I. A. (2008). Concentration of haemodynamic and inflammatory related cytokines in diabetic retinopathy. *Eye (Lond), 22*(2), 223-238. doi:10.1038/sj.eye.6702584

Ramin, S., Ahadi, M., & Ebrahimi, A. (2021). A study of therapeutic effects of 670 nm irradiation in different types of diabetic macular edema. *Biomed Photon, 9*(4), 15-22. doi:10.24931/2413-9432-2020-9-4-15-22

Roder, P. V., Wu, B., Liu, Y., & Han, W. (2016). Pancreatic regulation of glucose homeostasis. *Exp Mol Med, 48*(3), e219. doi:10.1038/emm.2016.6

Rubsam, A., Parikh, S., & Fort, P. E. (2018). Role of inflammation in DR. *Int J Mol Sci, 19*(4), 942. doi:10.3390/ijms19040942

Saliba, A., Du, Y., Liu, H., Patel, S., Roberts, R., Berkowitz, B. A., & Kern, T. S. (2015). Photobiomodulation mitigates diabetes-induced retinopathy by direct and indirect mechanisms: evidence from intervention studies in pigmented mice. *PLoS One, 10*(10), e0139003. doi:10.1371/journal.pone.0139003

Saltiel, A. R., & Kahn, C. R. (2001). Insulin signalling and the regulation of glucose and lipid metabolism. *Nature, 414*(6865), 799-806. doi:10.1038/414799a

Semeraro, F., Morescalchi, F., Cancarini, A., Russo, A., Rezzola, S., & Costagliola, C. (2019). Diabetic retinopathy, a vascular and inflammatory disease: Therapeutic implications. *Diabetes Metab, 45*(6), 517-527. doi:10.1016/j.diabet.2019.04.002

Sheibani, N., Sorenson, C. M., Cornelius, L. A., & Frazier, W. A. (2000). Thrombospondin-1, a natural inhibitor of angiogenesis, is present in vitreous and aqueous humor and is modulated by hyperglycemia. *Biochem Biophys Res Commun, 267*(1), 257-261. doi:10.1006/bbrc.1999.1903

Shen, W., Fruttiger, M., Zhu, L., Chung, S. H., Barnett, N. L., Kirk, J. K., . . . Gillies, M. C. (2012). Conditional Müllercell ablation causes independent neuronal and vascular pathologies in a novel transgenic model. *J Neurosci, 32*(45), 15715-15727. doi:10.1523/JNEUROSCI.2841-12.2012

Shimura, M., Yasuda, K., Nakazawa, T., Kano, T., Ohta, S., & Tamai, M. (2003). Quantifying alterations of macular thickness before and after panretinal photocoagulation in patients with severe diabetic retinopathy and good vision. *Ophthalmology, 110*(12), 2386-2394. doi:10.1016/j.ophtha.2003.05.008

Simo, R., Carrasco, E., Garcia-Ramirez, M., & Hernandez, C. (2006). Angiogenic and antiangiogenic factors in proliferative diabetic retinopathy. *Curr Diabetes Rev, 2*(1), 71-98. doi:10.2174/157339906775473671

Stenina, O. I., Krukovets, I., Wang, K., Zhou, Z., Forudi, F., Penn, M. S., . . . Plow, E. F. (2003). Increased expression of thrombospondin-1 in vessel wall of diabetic Zucker rat. *Circulation, 107*(25), 3209-3215. doi:10.1161/01.CIR.0000074223.56882.97

Stitt, A. W., Curtis, T. M., Chen, M., Medina, R. J., McKay, G. J., Jenkins, A., . . . Lois, N. (2016). The progress in understanding and treatment of diabetic retinopathy. *Prog Retin Eye Res, 51*, 156-186. doi:10.1016/j.preteyeres.2015.08.001

Symeonidis, C., Papakonstantinou, E., Androudi, S., Rotsos, T., Diza, E., Brazitikos, P., . . . Dimitrakos, S. A. (2011). Interleukin-6 and the matrix metalloproteinase response in the vitreous during proliferative vitreoretinopathy. *Cytokine, 54*(2), 212-217. doi:10.1016/j.cyto.2011.02.001

Tan, W., Zou, J.-L., Yoshida, S., Jiang, B., & Zhou, Y.-D. (2020). Increased vitreal levels of interleukin-10 in diabetic retinopathy: a Meta-analysis. *Int J Ophthalmol, 13*(9), 1477-1483. doi:10.18240/ijo.2020.09.21

Tang, J., Du, Y., Lee, C. A., Talahalli, R., Eells, J. T., & Kern, T. S. (2013). Low-intensity far-red light inhibits early lesions that contribute to diabetic retinopathy: in vivo and in vitro. *Invest Ophthalmol Vis Sci, 54*(5), 3681-3690. doi:10.1167/iovs.12-11018

Tang, J., Herda, A. A., & Kern, T. S. (2014). Photobiomodulation in the treatment of patients with non-center-involving diabetic macular oedema. *Br J Ophthalmol, 98*(8), 1013-1015. doi:10.1136/bjophthalmol-2013-304477

Tezel, G., & Wax, M. B. (2000). Increased production of tumor necrosis factor-alpha by glial cells exposed to simulated ischemia or elevated hydrostatic pressure induces apoptosis in cocultured retinal ganglion cells. *J Neurosci, 20*(23), 8693-8700. doi:10.1523/JNEUROSCI.20-23-08693.2000

Tsai, T., Kuekn, S., Tsiampalis, N., Vu, M.-K., Kakkassery, V., Stute, G., . . . Joachim, S. C. (2018). Anti-inflammatory cytokine and angiogenic factors levels in vitreous samples of diabetic retinopathy patients. *PLoS One, 13*(3), e0194603. doi:10.1371/journal.pone.0194603

Vecino, E., Rodriguez, F. D., Ruzafa, N., Pereiro, X., & Sharma, S. C. (2016). Glia-neuron interactions in the mammalian retina. *Prog Retin Eye Res, 51*, 1-40. doi:10.1016/j.preteyeres.2015.06.003

Vincent, J. A., & Mohr, S. (2007). Inhibition of caspase-1/interleukin-1beta signaling prevents degeneration of retinal capillaries in diabetes and galactosemia. *Diabetes, 56*(1), 224-230. doi:10.2337/db06-0427

Wahab, N. A., Schaefer, L., Weston, B. S., Yiannikouris, O., Wright, A., Babelova, A., . . . Mason, R. M. (2005). Glomerular expression of thrombospondin-1, transforming growth factor beta and connective tissue growth factor at different stages of diabetic nephropathy and their interdependent roles in mesangial response to diabetic stimuli. *Diabetologia, 48*(12), 2650-2660. doi:10.1007/s00125-005-0006-5

Wang, S., Gottlieb, J. L., Sorenson, C. M., & Sheibani, N. (2009). Modulation of thrombospondin 1 and pigment epithelium-derived factor levels in vitreous fluid of patients with diabetes. *Arch Ophthalmol, 127*(4), 507-513. doi:10.1001/archophthalmol.2009.53

Wang, X., Wang, G., & Wang, Y. (2009). Intravitreous vascular endothelial growth factor and hypoxia-inducible factor 1a in patients with proliferative diabetic retinopathy. *Am J Ophthalmol, 148*(6), 883-889. doi:10.1016/j.ajo.2009.07.007

Wilcox, G. (2005). Insulin and insulin resistance. *Clin Biochem Rev, 26*(2), 19-39.

Witmer, A. N., Vrensen, G. F., Van Noorden, C. J., & Schlingemann, R. O. (2003). Vascular endothelial growth factors and angiogenesis in eye disease. *Prog Retin Eye Res, 22*(1), 1-29. doi:10.1016/s1350-9462(02)00043-5

Wu, H., Hwang, D.-K., Song, X., & Tao, Y. (2017). Association between aqueous cytokines and diabetic retinopathy stage. *J Ophthalmol, 2017*, 9402198. doi:10.1155/2017/9402198

Wu, H., Hwang, D.-K., Song, X., & Tao, Y. (2017). Association between aqueous cytokines and diabetic retinopathy stage. *J Ophthalmol, 2017*, 9402198. doi:10.1155/2017/9402198

Wyble, C. W., Hynes, K. L., Kuchibhotla, J., Marcus, B. C., Hallahan, D., & Gewertz, B. L. (1997). TNF-α and IL-1 upregulate membrane-bound and soluble E-selectin through a common pathway. *J Surg Res, 73*(2), 107-112. doi:10.1006/jsre.1997.5207

Xing, T., Wang, Y., Ding, W.-J., Li, Y.-L., Hu, X.-D., Wang, C., . . . Shen, J.-L. (2017). Thrombospondin-1 production regulates the inflammatory cytokine secretion in THP-1 cells through NF-κB signaling pathway. *Inflammation, 40*(5), 1606-1621. doi:10.1007/s10753-017-0601-x

Yafai, Y., Eichler, W., Iandiev, I., Unterlauft, J.-D., Lochmann, C., Wiedemann, P., & Bringmann, A. (2014). Thrombospondin-1 is produced by retinal glial cells and inhibits the growth of vascular endothelial cells. *Ophthalmic Res, 52*(2), 81-88. doi:10.1159/000362371

Ye, E.-A., & Steinle, J. J. (2017). miR-146a suppresses STAT3/VEGF pathways and reduces apoptosis through IL-6 signaling in primary human retinal microvascular endothelial cells in high glucose conditions. *Vision Res, 139*, 15-22. doi:10.1016/j.visres.2017.03.009

Yoshida, S., Sotozono, C., Ikeda, T., & Kinoshita, S. (2001). Interleukin-6 (IL-6) production by cytokine-stimulated human Müller cells. *Curr Eye Res, 22*(5), 341-347. doi:10.1076/ceyr.22.5.341.5498

Yuuki, T., Kanda, T., Kimura, Y., Kotajima, N., Tamura, J., Kobayashi, I., & Kishi, S. (2001). Inflammatory cytokines in vitreous fluid and serum of patients with diabetic vitreoretinopathy. *J Diabetes Complications, 15*(5), 257-259. doi:10.1016/s1056-8727(01)00155-6

Zhang, H., Feng, Y.-W., & Yao, Y.-M. (2018). Potential therapy strategy: targeting mitochondrial dysfunction in sepsis. *Mil Med Res, 5*(1), 41. doi:10.1186/s40779-018-0187-0

Zhang, X., Zeng, H., Bao, S., Wang, N., & Gillies, M. C. (2014). Diabetic macular edema: new concepts in patho-physiology and treatment. *Cell Biosci, 4*, 27. doi:10.1186/2045-3701-4-27

Zhao, Y., & Singh, R. P. (2018). The role of anti-vascular endothelial growth factor (anti-VEGF) in the management of proliferative diabetic retinopathy. *Drugs Context, 7*, 212532. doi:10.7573/dic.212532

Zheng, L., Howell, S. J., Hatala, D. A., Huang, K., & Kern, T. S. (2007). Salicylate-based anti-inflammatory drugs inhibit the early lesion of diabetic retinopathy. *Diabetes, 56*(2), 337-345. doi:10.2337/db06-0789

Zhou, R., Horai, R., Mattapallil, M. J., & Caspi, R. R. (2011). A new look at immune privilege of the eye: dual role for the vision-related molecule retinoic acid. *J Immunol, 187*(8), 4170-4177. doi:10.4049/jimmunol.1101634

Zisman, A., Peroni, O. D., Abel, E. D., Mauvais-Jarvis, F., Lowell, B. B., Wojtaxzewski, J. F., . . . Kahn, B. B. (2000). Targeted disruption of the glucose transporter 4 selectively in muscle causes insulin resistance and glucose intolerance. *Nat Med, 6*(8), 924-928. doi:10.1038/78693

Zisman, A., Peroni, O. D., Abel, E. D., Mauvais-Jarvis, F., Lowell, B. B., Wojtaxzewski, J. F., . . . Kahn, B. B. (2000). Targeted disruption of the glucose transporter 4 selectively in muscle causes insulin resistance and glucose intolerance. *Nat Med, 6*(8), 924-928. doi:10.1038/78693

SUPPLEMENTARY FIGURES

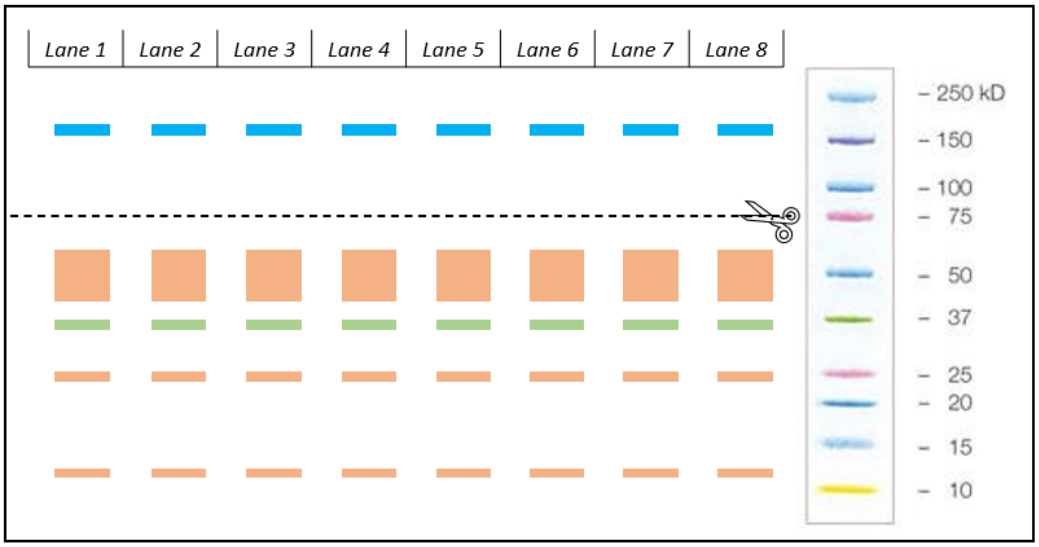

Supplementary Figure 1: Membrane layout and expected protein locations. *The anti-TSP-1 antibody data sheet indicated that various forms of the extracellular protein could be found at 165 – 198 kDa (teal), while the smaller 37 kDa GAPDH protein was expected to migrate further down the gel (green). The TGF-β protein monomer (12 kDa), dimer (25 kDa), and latent form (45 – 65 kDa) were also expected in the shown locations (orange). Western blot membranes were cut at 75 kDa after blocking to facilitate individual probing of primary antibodies.*

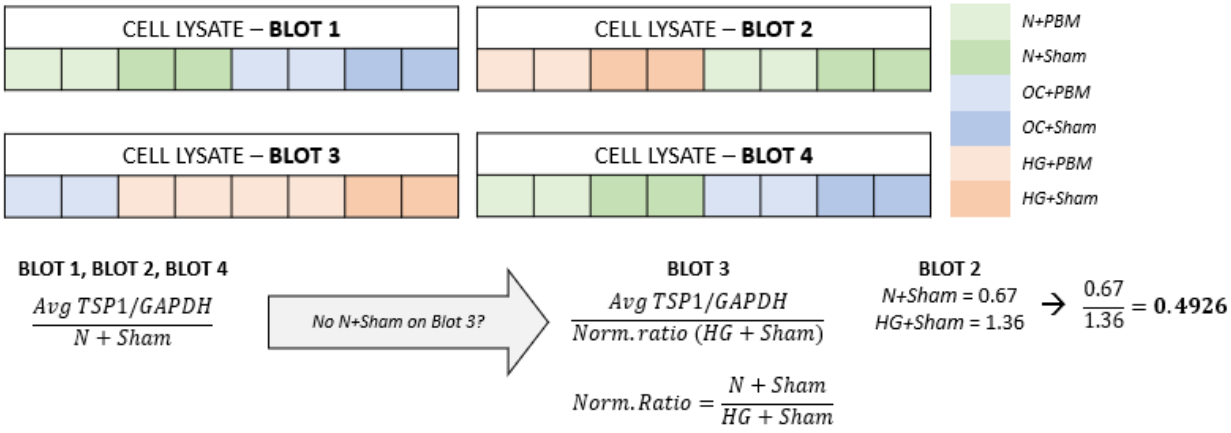

Supplementary Figure 2: Calculation of normalized TSP-1 values in cell lysate in absence of N+Sham on blot. *All blots corrected for well-to-well variation via normalization with GAPDH. Subsequent between blot variation required an identical sample on all four blots, which was not achieved. Blot 3 lacked N+Sham (dark green), so the value was approximated by determining the ratio of this group to HG+Sham (dark orange), a sample that did appear on the blot. In summary, blot 3 was normalized with HG+Sham. The resulting values were then multiplied by the normalizing ratio, 0.4926.*

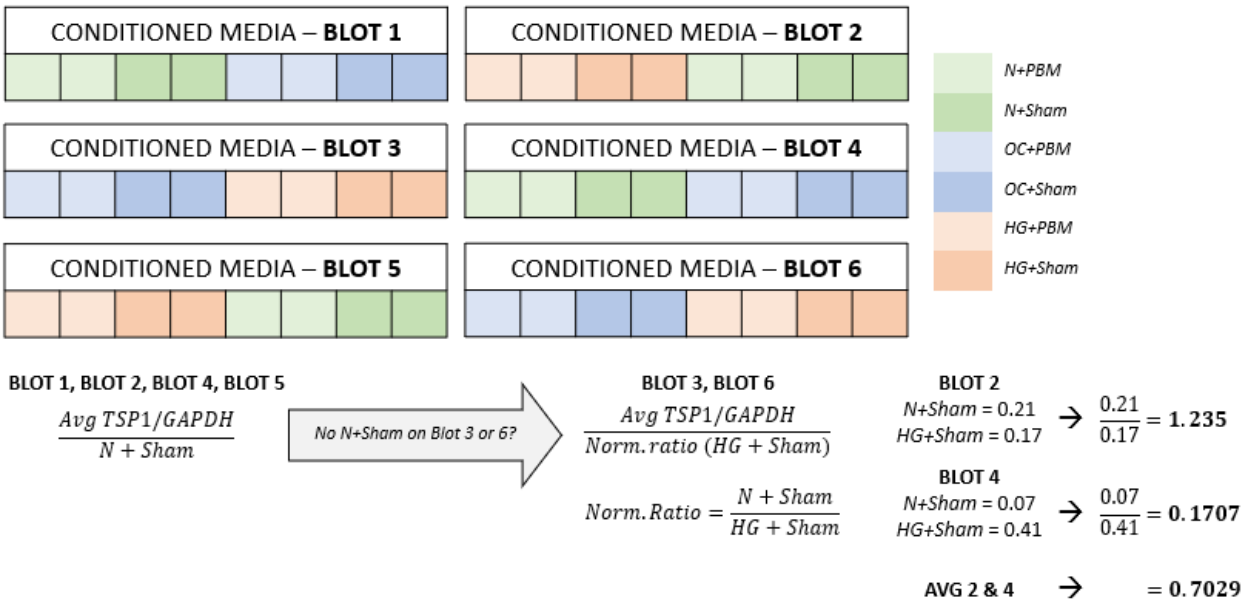

Supplementary Figure 3: Calculation of normalized TSP-1 values in muller cell conditioned media in absence of N+Sham on blot. *All blots corrected for well-to-well variation via normalization with total protein measurements gather with membrane staining. Subsequent between blot variation required an identical sample on all six blots, which was not achieved. Blots 3 and 6 lacked N+Sham (dark green), so the value was approximated by determining the ratio of this group to HG+Sham (dark orange), a sample that did appear on the blot. In summary, blots 3 and 6 were normalized with HG+Sham. There was a 7-fold difference between the high and low ratios, so each was separately used in TSP-1 calculations.*

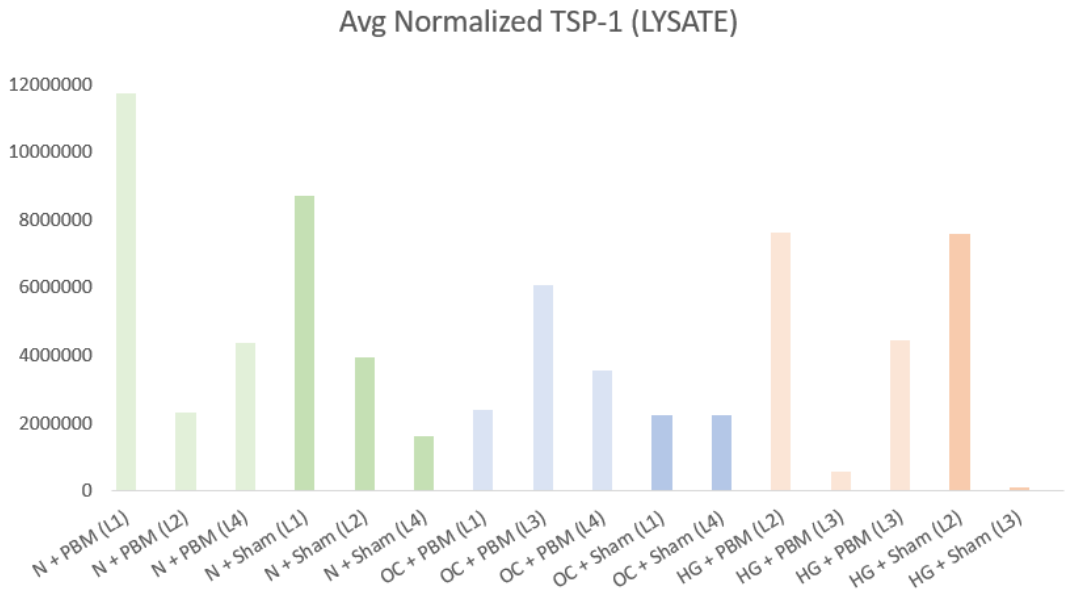

Supplementary Figure 4: Compiled relative quantities of TSP-1 in Muller cell lysate across blots. *TSP-1 signal normalized to housekeeping protein GAPDH. Y-axis represents chemiluminescent signal density. No inter-blot normalization. Each bar represents a duplicate average. L# = lysate blot number.*

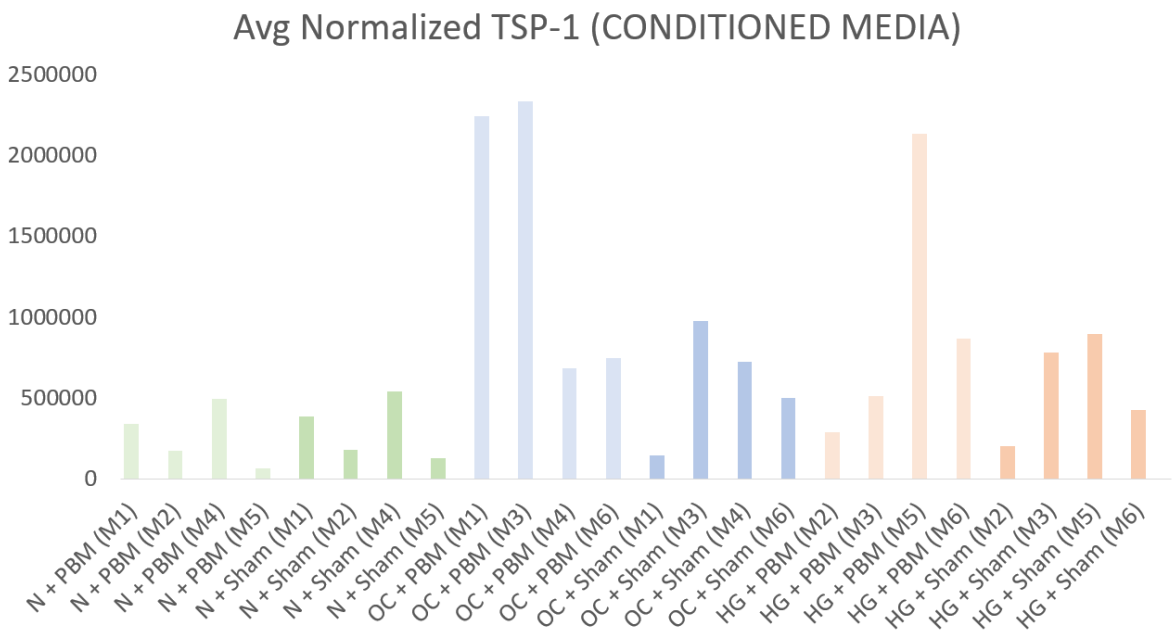

Supplementary Figure 5: Compiled relative quantities of TSP-1 in Muller cell conditioned media across blots. *TSP-1 signal normalized to total protein. Y-axis represents chemiluminescent signal density. No inter-blot normalization. Each bar represents a duplicate average. M# = media blot number.*

	1	2	3	4	5	6	7	8	9	10	11	12
A	Std 1	Std 1	T11A conc med 1:1	T11A conc med 1:5	T11A conc med 1:10	T23A conc med 1:1	T23A conc med 1:5	T23A conc med 1:10	T34A conc med 1:1	T34A conc med 1:5	T34A conc med 1:10	
B	Std 2	Std 2	T11B conc med 1:1	T11B conc med 1:5	T11B conc med 1:10	T23B conc med 1:1	T23B conc med 1:5	T23B conc med 1:10	T34B conc med 1:1	T34B conc med 1:5	T34B conc med 1:10	
C	Std 3	Std 3	T13A conc med 1:1	T13A conc med 1:5	T13A conc med 1:10	T24A conc med 1:1	T24A conc med 1:5	T24A conc med 1:10	T41A conc med 1:1	T41A conc med 1:5	T41A conc med 1:10	
D	Std 4	Std 4	T13B conc med 1:1	T13B conc med 1:5	T13B conc med 1:10	T24B conc med 1:1	T24B conc med 1:5	T24B conc med 1:10	T41B conc med 1:1	T41B conc med 1:5	T41B conc med 1:10	
E	Std 5	Std 5	T14A conc med 1:1	T14A conc med 1:5	T14A conc med 1:10	T31A conc med 1:1	T31A conc med 1:5	T31A conc med 1:10	T43A conc med 1:1	T43A conc med 1:5	T43A conc med 1:10	
F	Std 6	Std 6	T14B conc med 1:1	T14B conc med 1:5	T14B conc med 1:10	T31B conc med 1:1	T31B conc med 1:5	T31B conc med 1:10	T43B conc med 1:1	T43B conc med 1:5	T43B conc med 1:10	
G	Std 7	Std 7	T21A conc med 1:1	T21A conc med 1:5	T21A conc med 1:10	T33A conc med 1:1	T33A conc med 1:5	T33A conc med 1:10	T44A conc med 1:1	T44A conc med 1:5	T44A conc med 1:10	
H	Std 8	Std 8	T21B conc med 1:1	T21B conc med 1:5	T21B conc med 1:10	T33B conc med 1:1	T33B conc med 1:5	T33B conc med 1:10	T44B conc med 1:1	T44B conc med 1:5	T44B conc med 1:10	

Supplementary Figure 6: Luminex MAGPIX assay 96-well plate layout. *Conditioned media samples were run in triplicate at three dilutions (1:1, 1:5, 1:10).*

SUPPLEMENTARY TABLES

Supplementary Table 1: TSP-1 in cell lysate normalization in absence of N+Sham on blot. Sample labels indicate the trial number (T#), substrate group (Group 1 = normal glucose, Group 2 = mannitol, Group 3 = high glucose), and treatment (A = PBM, B = Sham).

Treatment & Blot #	Sample ID	TSP-1/GAPDH	Avg TSP-1/GAPDH	Avg TSP-1/GAPDH (norm. w/ HG+Sham)	Avg TSP-1/GAPDH (norm. w/ N+Sham)
N + PBM (L1)	T11A	1.18	1.11		1.30
	T11A	1.03			1.13
N + Sham (L1)	T11B	0.98	0.91		1.07
	T11B	0.85			0.93
OC + PBM (L1)	T13A	0.30	0.27		0.33
	T13A	0.24			0.27
OC + Sham (L1)	T13B	0.31	0.37		0.34
	T13B	0.44			0.48
N + PBM (L2)	T21A	0.33	0.42		0.49
	T21A	0.51			0.76
N + Sham (L2)	T21B	0.81	0.67		1.20
	T21B	0.54			0.80
HG + PBM (L2)	T14A	1.27	1.29		1.89
	T14A	1.30			1.93
HG + Sham (L2)	T14B	1.59	1.36		2.36
	T14B	1.12			1.67
OC + PBM (L3)	T23A	0.63	0.59	25.99	12.80
	T23A	0.54		22.35	11.01
HG + PBM (L3)	T24A	0.13	0.11	5.33	2.62
	T24A	0.09		3.56	1.75
HG + PBM (L3)	T34A	0.60	0.61	24.71	12.17
	T34A	0.63		25.81	12.71
HG + Sham (L3)	T24B	0.03	0.02	1.05	0.52
	T24B	0.02		0.95	0.47
N + PBM (L4)	T31A	0.40	0.46		2.04
	T31A	0.51			2.57
N + Sham (L4)	T31B	0.20	0.20		1.00
	T31B	0.20			1.00
OC + PBM (L4)	T33A	0.57	0.73		2.89
	T33A	0.88			4.48
OC + Sham (L4)	T33B	0.26	0.35		1.32
	T33B	0.45			2.28

Supplementary Table 2: TSP-1 in conditioned media normalization in absence of N+Sham on blot. *Sample labels indicate the trial number (T#), substrate group (Group 1 = normal glucose, Group 2 = mannitol, Group 3 = high glucose), and treatment (A = PBM, B = Sham).*

Treatment & Blot #	Sample ID	TSP-1/GAPDH	Avg TSP-1/GAPDH	Avg TSP-1/GAPDH (norm. w/ HG+Sham)	Avg TSP-1/GAPDH (norm. w/ N+Sham)
N + PBM (M1)	T11A	0.13	0.11		1.04
	T11A	0.10			0.79
N + Sham (M1)	T11B	0.08	0.12		0.66
	T11B	0.16			1.34
OC + PBM (M1)	T13A	2.51	1.28		20.46
	T13A	0.04			0.35
OC + Sham (M1)	T13B	0.08	0.05		0.65
	T13B	0.03			0.23
N + PBM (M2)	T21A	0.12	0.15		0.58
	T21A	0.18			0.82
N + Sham (M2)	T21B	0.23	0.21		1.10
	T21B	0.19			0.90
HG + PBM (M2)	T14A	0.17	0.15		0.79
	T14A	0.13			0.61
HG + Sham (M2)	T14B	0.17	0.17		0.81
	T14B	0.17			0.79
OC + PBM (M3)	T23A	1.01	1.07	2.08	2.57
	T23A	1.14		2.37	2.92
OC + Sham (M3)	T23B	0.48	0.49	0.99	1.23
	T23B	0.50		1.05	1.29
HG + PBM (M3)	T24A	0.30	0.26	0.63	0.78
	T24A	0.22		0.45	0.55
HG + Sham (M3)	T24B	0.36	0.48	0.75	0.93
	T24B	0.60		1.25	1.54
OC + PBM (M3)	T23A	1.01	1.07	2.08	0.36
	T23A	1.14		2.37	0.40
OC + Sham (M3)	T23B	0.48	0.49	0.99	0.17
	T23B	0.50		1.05	0.18
HG + PBM (M3)	T24A	0.30	0.26	0.63	0.11
	T24A	0.22		0.45	0.08
HG + Sham (M3)	T24B	0.36	0.48	0.75	0.13
	T24B	0.60		1.25	0.21
OC + PBM (M3)	T23A	1.01	1.07	2.08	1.47
	T23A	1.14		2.37	1.66
OC + Sham (M3)	T23B	0.48	0.49	0.99	0.70
	T23B	0.50		1.05	0.73
HG + PBM (M3)	T24A	0.30	0.26	0.63	0.44
	T24A	0.22		0.45	0.32
HG + Sham (M3)	T24B	0.36	0.48	0.75	0.53
	T24B	0.60		1.25	0.88

Supplementary Table 2 (continued): TSP-1 in conditioned media normalization in absence of N+Sham on blot. *Sample labels indicate the trial number (T#), substrate group (Group 1 = normal glucose, Group 2 = mannitol, Group 3 = high glucose), and treatment (A = PBM, B = Sham).*

Treatment & Blot #	Sample ID	TSP-1/GAPDH	Avg TSP-1/GAPDH	Avg TSP-1/GAPDH (norm. w/ HG+Sham)	Avg TSP-1/GAPDH (norm. w/ N+Sham)
N + PBM (M4)	T31A	0.19	0.22		0.75
	T31A	0.26			1.04
N + Sham (M4)	T31B	0.24	0.25		0.98
	T31B	0.25			1.02
OC + PBM (M4)	T33A	0.35	0.36		1.40
	T33A	0.37			1.47
OC + Sham (M4)	T33B	0.36	0.39		1.45
	T33B	0.42			1.70
N + PBM (M5)	T41A	0.03	0.03		0.46
	T41A	0.04			0.50
N + Sham (M5)	T41B	0.06	0.07		0.81
	T41B	0.08			1.19
HG + PBM (M5)	T34A	1.40	0.92		19.65
	T34A	0.44			6.14
HG + Sham (M5)	T34B	0.38	0.41		5.32
	T34B	0.44			6.23
OC + PBM (M6)	T43A	0.09	0.07	0.87	1.07
	T43A	0.05		0.51	0.63
OC + Sham (M6)	T43B	0.07	0.08	0.71	0.87
	T43B	0.08		0.72	0.89
HG + PBM (M6)	T44A	0.10	0.11	0.95	1.17
	T44A	0.12		1.14	1.41
HG + Sham (M6)	T44B	0.11	0.11	1.02	1.26
	T44B	0.10		0.98	1.21
OC + PBM (M6)	T43A	0.09	0.07	0.87	0.15
	T43A	0.05		0.51	0.09
OC + Sham (M6)	T43B	0.07	0.08	0.71	0.12
	T43B	0.08		0.72	0.12
HG + PBM (M6)	T44A	0.10	0.11	0.95	0.16
	T44A	0.12		1.14	0.19
HG + Sham (M6)	T44B	0.11	0.11	1.02	0.17
	T44B	0.10		0.98	0.17
OC + PBM (M6)	T43A	0.09	0.07	0.87	0.61
	T43A	0.05		0.51	0.36
OC + Sham (M6)	T43B	0.07	0.08	0.71	0.50
	T43B	0.08		0.72	0.51
HG + PBM (M6)	T44A	0.10	0.11	0.95	0.67
	T44A	0.12		1.14	0.80
HG + Sham (M6)	T44B	0.11	0.11	1.02	0.72
	T44B	0.10		0.98	0.69

Supplementary Table 3: Raw densitometry values of cell lysate western blots.									
Blot ID	*Protein*	*Lane 1*	*Lane 2*	*Lane 3*	*Lane 4*	*Lane 5*	*Lane 6*	*Lane 7*	*Lane 8*
LYSATE BLOT 1	TSP-1	13871250	10768446	10517250	8773750	3249150	2270750	2361150	3856350
	GAPDH	11725542	10482423	10785600	10382900	10814336	9284096	7656132	8835660
LYSATE BLOT 2	TSP-1	8379606	7685088	9566631	6894588	2116347	2948361	4268649	3975858
	GAPDH	6592026	5902022	6021594	6137132	6380140	5735744	5285412	7382298
LYSATE BLOT 3	TSP-1	6137985	5617507	5186797	5100753	1006068	555317	161063	168854
	GAPDH	9735612	10362180	8650993	8147694	7785505	6431400	6341048	7303225
LYSATE BLOT 3	TSP-1	4581600	4887550	2148450	1600250	4535389	6260228	2205682	3791991
	GAPDH	11366100	9625622	10859769	8136351	7950040	7083934	8484210	8440618

Supplementary Table 4: Raw densitometry values of conditioned media western blots.									
Blot ID	*Protein*	*Lane 1*	*Lane 2*	*Lane 3*	*Lane 4*	*Lane 5*	*Lane 6*	*Lane 7*	*Lane 8*
MEDIA BLOT 1	TSP-1	505653	256753	293744	571708	6576550	146450	276100	74050
	Swift	3950388	2643885	3619880	3479179	2618622	3418650	3456200	2665798
MEDIA BLOT 2	TSP-1	411318	226900	294112	288600	249900	251736	279628	326550
	Swift	2446528	1753794	1697190	1707100	2018876	1432080	1191296	1699314
MEDIA BLOT 3	TSP-1	2305773	2483650	1060100	1035200	656050	447200	587250	1260450
	Swift	2291460	2175156	2214072	2051554	2154515	2063670	1616576	2093268
MEDIA BLOT 4	TSP-1	444100	578950	570500	563750	735950	790300	798000	847700
	Swift	2395904	2238206	2349870	2222946	2114700	2161200	2216240	2014194
MEDIA BLOT 5	TSP-1	3353356	978450	891150	986250	68600	77000	128400	170200
	Swift	2395904	2238206	2349870	2222946	2114700	2161200	2216240	2014194
MEDIA BLOT 6	TSP-1	974882	548862	597924	667998	1026426	975120	696201	688245
	Swift	10610715	10106792	8000056	8703422	10230248	8079264	6453704	6611856

Supplementary Table 5: Effect of N+Sham/HG+Sham ratio on normalized TSP-1 in Muller cell conditioned media

N+Sham/HG+Sham Ratio: 1.235		N+Sham/HG+Sham Ratio: 0.1707		N+Sham/HG+Sham Ratio: 0.7029	
N + Sham	*N + PBM*	*N + Sham*	*N + PBM*	*N + Sham*	*N + PBM*
0.66	1.04	0.66	1.04	0.66	1.04
1.34	0.79	1.34	0.79	1.34	0.79
1.1	0.58	1.1	0.58	1.1	0.58
0.9	0.82	0.9	0.82	0.9	0.82
0.98	0.75	0.98	0.75	0.98	0.75
1.02	1.04	1.02	1.04	1.02	1.04
0.81	0.46	0.81	0.46	0.81	0.46
1.19	0.5	1.19	0.5	1.19	0.5

N+Sham/HG+Sham Ratio: 1.235		N+Sham/HG+Sham Ratio: 0.1707		N+Sham/HG+Sham Ratio: 0.7029	
OC + Sham	*OC + PBM*	*OC + Sham*	*OC + PBM*	*OC + Sham*	*OC + PBM*
0.65	20.46	0.65	20.46	0.65	20.46
0.23	0.35	0.23	0.35	0.23	0.35
1.23	2.57	0.17	0.36	0.7	1.47
1.29	2.92	0.18	0.4	0.73	1.66
1.45	1.4	1.45	1.4	1.45	1.4
1.7	1.47	1.7	1.47	1.7	1.47
0.87	1.07	0.12	0.15	0.5	0.61
0.89	0.63	0.12	0.09	0.51	0.36

N+Sham/HG+Sham Ratio: 1.235		N+Sham/HG+Sham Ratio: 0.1707		N+Sham/HG+Sham Ratio: 0.7029	
HG + Sham	*HG + PBM*	*HG + Sham*	*HG + PBM*	*HG + Sham*	*HG + PBM*
0.81	0.79	0.81	0.79	0.81	0.79
0.79	0.61	0.79	0.61	0.79	0.61
0.93	0.78	0.13	0.11	0.53	0.44
1.54	0.55	0.21	0.08	0.88	0.32
5.32	19.65	5.32	19.65	5.32	19.65
6.23	6.14	6.23	6.14	6.23	6.14
1.26	1.17	0.17	0.16	0.72	0.67
1.21	1.41	0.17	0.19	0.69	0.8

Supplementary Table 6: Protein Expression in Diabetic Retinopathy. *PDR-NG = proliferative diabetic retinopathy with neovascular glaucoma.*

Protein	*Model*	*Sample*	*Finding (compared to controls unless specified)*	*Detection Method*	*Paper*
IL-1β	Rats (STZ)	Retina	↑ expression	Western blot	(Kowluru & Odenbach, 2004)
IL-1β	Mice (STZ)	Retina	↑ expression	ELISA	(Vincent & Mohr, 2007)
IL-1β	DR patients	Aqueous humor	↑ in PDR and NPDR patients	Cytometric bead assay	(Wu, Hwang, Song, & Tao, 2017)
IL-1β	DR patients	Aqueous humor	No sig changes in PDR and NPDR patients	Cytometric bead assay	(Chen, Zhang, Liao, & Wen, 2017)
IL-1β	DR patients	Vitreous	↑ in PDR patients, but not NPDR patients	ELISA	(Patel, Saleh, Hykin, Gregor, & Cree, 2008)
IL-1β	DR patients	Vitreous	↑ in PDR and NPDR patients	ELISA	(Chen, et al., 2018)
IL-1β	DR patients	Vitreous	↑ in PDR patients (NPDR not examined)	ELISA	(Demircan, Safran, Soylu, Ozcan, & Sizmaz, 2006)
IL-1β	DR patients	Vitreous	↑ in DR patients	ELISA	(Tsai, et al., 2018)
IL-1β	DR patients	Vitreous	↑ in PDR patients (NPDR not examined)	ELISA	(Mao & Yan, 2014)
IL-1β	DR patients	Vitreous	No sig changes in expression between PDR or NPDR groups	ELISA	(Loukovaara, et al., 2017)
IL-1β	DR patients	Vitreous	No sig changes in PDR patients (NPDR not examined)	ELISA	(Loporchio, et al., 2021)
IL-1β	DR patients	PBMC culture supernatant	↑ in PDR and NPDR patients	ELISA	(Chen, et al., 2018)
IL-1β	DR patients	PBMCs	↑ in PDR and NPDR patients	RT-PCR	(Chen, et al., 2018)
IL-1β	DR patients	Serum	↑ in PDR patients (NPDR not examined)	ELISA	(Demircan, Safran, Soylu, Ozcan, & Sizmaz, 2006)
IL-6	DR patients	Aqueous humor	↑ in PDR and NPDR patients	Cytometric bead assay	(Wu, Hwang, Song, & Tao, 2017)
IL-6	DR patients	Aqueous humor	↑ in PDR and NPDR patients	Cytometric bead assay	(Chen, Zhang, Liao, & Wen, 2017)
IL-6	DR patients	Aqueous humor	↑ concentration with disease severity (NPDR → PDR → PDR-NG; no controls)	?	(Song, Yu, Zhang, & Dai, 2020)
IL-6	DR patients	Vitreous	No sig changes in expression between PDR or NPDR groups	ELISA	(Loukovaara, et al., 2017)

IL-6	DR patients	Vitreous	↑ in PDR patients (NPDR not examined)	ELISA	(Yuuki, et al., 2001)
IL-6	DR patients	Vitreous	No sig change in DR patients	ELISA	(Tsai, et al., 2018)
IL-6	DR patients	Vitreous	No sig changes in PDR patients (NPDR not examined)	ELISA	(Loporchio, et al., 2021)
IL-6	DR patients	Serum	No sig changes in PDR patients	ELISA	(Yuuki, et al., 2001)
TNF-α	Rats (STZ)	Retina	↑ expression	ELISA	(Joussen, et al., 2002)
TNF-α	DR patients	Aqueous humor	↑ in PDR and NPDR patients	Cytometric bead assay	(Wu, Hwang, Song, & Tao, 2017)
TNF-α	DR patients	Aqueous humor	No sig changes in PDR or NPDR patients	Cytometric bead assay	(Chen, Zhang, Liao, & Wen, 2017)
TNF-α	DR patients	Vitreous	No sig change in expression between PDR or NPDR groups	ELISA	(Loukovaara, et al., 2017)
TNF-α	DR patients	Vitreous	No sig changes in PDR patients (NPDR not examined)	ELISA	(Yuuki, et al., 2001)
TNF-α	DR patients	Vitreous	No sig changes in PDR patients (NPDR not examined)	ELISA	(Loporchio, et al., 2021)
TNF-α	DR patients	Vitreous	↑ in PDR patients (NPDR not examined)	ELISA	(Demircan, Safran, Soylu, Ozcan, & Sizmaz, 2006)
TNF-α	DR patients	Vitreous	↑ in PDR patients (NPDR not examined)	Various (meta-analysis)	(McAuley, et al., 2014)
TNF-α	DR patients	Serum	↑ in PDR patients (NPDR not examined)	ELISA	(Demircan, Safran, Soylu, Ozcan, & Sizmaz, 2006)
TNF-α	DR patients	Serum	↑ in PDR patients (NPDR not examined)	ELISA	(Yuuki, et al., 2001)
TNF-α	DR patients	Serum	↑ in PDR patients (NPDR not examined)	Various (meta-analysis)	(Yao, et al., 2018)
IL-10	DR patients	Aqueous humor	↑ in PDR (not NPDR)	Cytometric bead assay	(Wu, Hwang, Song, & Tao, 2017)
IL-10	DR patients	Aqueous humor	No sig changes in PDR or NPDR patients	Cytometric bead assay	(Chen, Zhang, Liao, & Wen, 2017)
IL-6	DR patients	Aqueous humor	↑ concentration with disease severity (NPDR → PDR → PDR-NG; no controls)	?	(Song, Yu, Zhang, & Dai, 2020)
IL-10	DR patients	Vitreous	↑ in PDR patients (NPDR not examined)	ELISA	(Mao & Yan, 2014)
IL-10	DR patients	Vitreous	↑ in DR patients	Various (meta-analysis)	(Tan, Zou, Yoshida, Jiang, & Zhou, 2020)
IL-10	DR patients	Vitreous	No sig changes in PDR patients (NPDR not examined)	ELISA	(Loporchio, et al., 2021)

TSP-1	DM patients	Vitreous	↓ expression	Western blot	(Wang, Gottlieb, Sorenson, & Sheibani, 2009)
TSP-1	Rats (STZ)	Aqueous humor	↓ expression	Western blot	(Sheibani, Sorenson, Cornelius, & Frazier, 2000)
TSP-1	Rats (STZ)	Vitreous	↓ expression	Western blot	(Sheibani, Sorenson, Cornelius, & Frazier, 2000)
TSP-1	Rats (STZ)	Retina	↑ expression	RT-PCR	(Wang, Zhang, & Zhang, 2006)
TGF-β	DR patients	Vitreous	↑ in PDR (NPDR not examined)	Cytometric bead assay	(Dai, Wu, Wang, Zhang, & Yu, 2014)
TGF-β	DR patients	Vitreous	↑ in PDR (NPDR not examined)	ELISA	(Hirase, et al., 1998)
TNF-α	DR patients	Vitreous	↑ in PDR patients (NPDR not examined)	Various (meta-analysis)	(McAuley, et al., 2014)
TGF-β	DR patients	Aqueous humor	↑ concentration with disease severity (NPDR → PDR → PDR-NG; no controls)	?	(Song, Yu, Zhang, & Dai, 2020)